Phenotypic and *omics* analyses of the Sordariomycetes *Marquandomyces marquandii* and *Albophoma yamanashiensis* isolated from estuarine sediments.

Z. Agirrezabala[1], A. Otamendi[1], R. Liébana[2], M. Azkargorta[3], C. Perez-Cruz[2], M. T. Dueñas[1], M. Ostra[4], R. López[5], I.V. Grigoriev[6,7], L. Alonso-Sáez[2], F. Elortza[3], A. Lanzén[8,9], S. Haridas[6], Oier Etxebeste[1,#]

[1]*Laboratory of Microbiology, Dept. of Applied Chemistry, Faculty of Chemistry, University of the Basque Country (UPV/EHU), 20018 San Sebastian.*

[2]*AZTI, Marine Research, Basque Research and Technology Alliance (BRTA), Sukarrieta.*

[3]*Proteomics Platform, Center for Cooperative Research in Biosciences (CIC bioGUNE), Basque Research and Technology Alliance (BRTA), CIBERehd, 48160, Derio.*

[4]*Laboratory of Analytical Chemistry, Dept. of Applied Chemistry, Faculty of Chemistry, University of the Basque Country (UPV/EHU), 20018 San Sebastian.*

[5]*Dept. of Organic Chemistry I, Faculty of Chemistry, University of the Basque Country (UPV/EHU), 20018 San Sebastian.*

[6]*U.S. Department of Energy Joint Genome Institute (JGI), Lawrence Berkeley National Laboratory, Berkeley, CA 94720, USA.*

[7]*Department of Plant and Microbial Biology, University of California Berkeley, Berkeley, CA 94720, USA.*

[8]*AZTI, Marine Research, Basque Research and Technology Alliance (BRTA), Pasaia.*

[9]*IKERBASQUE, Basque Foundation for Science, Bilbao.*

[≠] Corresponding author: E-mail: oier.echeveste@ehu.eus; Tel: (+34)943018517; Fax: (+34)943015270; Lab. of Biology, Dept. of Applied Chemistry, Faculty of Chemistry, University of the Basque Country, Manuel de Lardizabal, 3, 20018, San Sebastian.

Abstract.

Marine environments harbor a vast diversity of microorganisms, which have developed multiple strategies to adapt to challenging conditions and represent a valuable source for new products such as pigments, enzymes and bioactive compounds. From all microorganisms inhabiting marine environments, fungi have been the least studied, despite their ubiquitous presence and great biotechnological potential. Here, we focused on the isolation and characterization of filamentous fungi from marine sediment samples, which were collected along the Basque coast in Spain. Through phenotypic characterization, we identified isolates potentially able to produce secondary metabolites or grow on minimal culture medium supplemented with recalcitrant algal polysaccharides. Based on this screening, two Sordariomycetes isolates were selected for further analyses through genome sequencing and *omics* techniques: 1) a *Marquandomyces marquandii* strain able to stain the culture medium in yellow, indicative of secretion of pigments and secondary metabolites and 2) an *Albophoma yamanashiensis* strain able to grow in minimal culture medium supplemented with the recalcitrant algal polysaccharide fucoidan. Fungal co-culture experiments suggested an inhibitory effect of the secretome of *M. marquandii* on fungal growth. Under culture conditions inducing pigment secretion, a set of secondary metabolite gene clusters were differentially expressed, as analysed by RNA-seq. On the other hand, transcriptomic and proteomic experiments on *A. yamanashiensis* unveiled the enzymatic activities expressed in response to the presence of fucoidan. Overall, our results indicate that the isolated marine fungal strains could serve as a source of new enzymatic activities and secondary metabolites.

Keywords. Estuarine filamentous fungi; Sordariomycetes; Hypocreales; CAZYmes; secondary metabolite gene clusters; secondary metabolites; fucoidan.

1. Introduction.

Fungi probably represent the largest and most diverse eukaryotic kingdom, with an estimated number of species ranging from 2 to 3 million [1–4]. They have adapted to very diverse environments and niches [5], including high salt concentrations, nutrient limitation, or environments where the main source of carbon and nitrogen is in form of recalcitrant polymers. The first marine fungal strains were isolated more than a century ago [6] and research interest on marine mycology has grown considerably in the last years. However, the state-of-the-art in this field lags behind that of other microorganisms such as marine bacteria. As a reference, the number of total marine fungal species listed in the Marine Fungi website (https://www.marinefungi.org/; [7]) is 2,149, as of February 2025. In contrast, the bacterial database BacDive [8] includes a subset of 7,916 strains with the tag "*aquatic*", 2,040 strains with the tag "*marine*" and 1,550 strains with the tag "*sediment*" (accessed in October 2024). Based on metabarcoding analyses, it is hypothesized that the number of marine fungal species and their diversity is far larger than the number of species currently deposited in culture collections [6,9,10]. One of the reasons explaining this gap is the difficulty for cultivating slow-growing marine fungi under laboratory conditions [11]. Overall, it can be concluded that the potential impact of fungi at environmental and biotechnological levels is underestimated [6,12].

Genome sequencing of cultivable marine fungal strains has revealed biotechnological potential in several fields, such as the identification of compounds with antitumoral activity as well as new antimicrobials, pigments and other secondary metabolites [13]. Fungal secondary metabolites are compounds of different types, such as polyketides, terpenes, non-ribosomal peptides (NRPs), ribosomally synthesized and post-

translationally modified peptides or RiPPs, which confer advantages in particular niches [14]. Their synthesis, modification, cellular compartmentalization, and secretion are encoded in the genome by groups of genes that are typically located in clusters. Elucidating the genetic mechanisms controlling the expression of these secondary metabolite gene clusters and the chemical reactions catalyzed by their activities is key for the identification of new bioactive compounds and the optimization of their industrial synthesis.

Marine fungal strains capable of degrading polysaccharides of marine origin have also been identified [13,15,16], which are of interest in biotechnology. Marine polysaccharides, synthesized by phytoplankton and macroalgae during photosynthesis, exhibit a great diversity of chemical structures, in terms of monosaccharide composition, linkage types and decoration patterns [17]. Among these, fucoidans are complex algal polysaccharides mainly composed of fucose, typically branched and heavily sulfated, which confers them negative charges. The degradation of these complex molecules involves a coordinated action of Carbohydrate-Active enZymes (CAZymes) and sulfatases [18]. CAZymes, including glycoside hydrolases (GHs), carbohydrate esterases (CEs), and polysaccharide lyases (PLs) break down fucoidan by hydrolyzing glycosidic bonds, while sulfatases remove sulfate groups to facilitate further degradation. Notably, the knowledge on the ability of marine fungi to degrade fucoidan and the molecular mechanisms employed is still very limited. Discovering new enzymes with novel catalytic activities modifying and breaking down fucoidan is of great interest, since these polysaccharides and the oligosaccharides resulting from their partial degradation have shown immunomodulatory, anti-inflammatory, virucidal or anticancer activities [19–23].

In this work, we focused on the isolation of filamentous fungi from sediment samples collected in five estuaries of the Basque Country (Bay of Biscay). From the resulting library of isolates, mainly formed by Sordariomycetes and Eurotiomycetes fungi, we focused our analysis on isolate M60 (*Marquandomyces marquandii*) based on its ability to produce and secrete pigments, which may be used in the food, cosmetic and textile sectors [24]; and M98 (*Albophoma yamanshiensis*), due to its phenotype on culture medium supplemented with polysaccharides of marine origin. Results of phenotypic and *omics* analyses of both isolates strongly suggest that the isolates of our library could serve as a source of new enzymatic activities and secondary metabolites.

2. Experimental.

2.1. Sample collection, processing and isolation of filamentous fungi.

Seven stations along the Basque coast (Bay of Biscay) were selected for sampling (Figure 1). The selected samples covered diverse values of organic content and granulometry properties. One of these stations (LUR20) is located approximately 0.8 km from the coast, at a depth of 37 m (black square in Figure 1). Samples were collected during winter and spring of 2021, in 50 mL polypropylene tubes, which were stored at 4 ºC until processing.

For isolation of fungi, the *dilution-to-extinction* method was used [11] based on the procedure developed by Velez and coworkers [25]. Briefly, approximately two centimeters of the upper layer of the sediment were removed using a sterile spatula. Samples of 1.4-2.2 g were taken from the center of each tube (material that was not in contact with the wall of the tube) and transferred to 15 mL polypropylene tubes. Sediment samples were diluted serially (1/5 once and 1/10 twice) in artificial sea water (ASW; see below). Aliquots of 50 µL per well were inoculated in 24-well plates

previously filled with the culture medium (see below) plus penicillin. One well per plate was inoculated with ASW as a control for potential contaminations. Plates were covered with aluminum foil and cultured under aerobic conditions at atmospheric pressure and 25º C. Growth was checked regularly and samples of isolates generating filaments were transferred to plates containing the same culture medium used for isolation, until homogeneous phenotypes, and thus probably axenic cultures, were obtained. Specific isolates showed invasive behavior and colonized adjacent wells in multi-well plates. To minimize contamination, these isolates were discarded from the analysis. Samples of all selected isolates were stored at -80º C in a glycerol solution (18% in artificial seawater).

2.2. Preparation of culture media and solutions.

ASW solutions were prepared by diluting 90 g of sea salts (Millipore) per liter of distilled water (3x stock; 9%; ASW1) [15]. Alternatively, a 4x stock (ASW2) was prepared by adding 46.94 g NaCl, 7.84 g Na_2SO_4, 21.28 g $MgCl_2{\cdot}6H_2O$, 2.20 g $CaCl_2$, 0.38 g $NaHCO_3$, 1.33 g KCl, 0.19 g KBr, 0.05 g H_3BO_3, 0.05 g $SrCl_2$ and 0.006 g NaF per liter of distilled water [26]. Penicillin sodium salt (0.018 mg/mL; 30 units/mL) was added to all culture media used for isolation. Six types of media carrying different carbon and nitrogen sources were used for isolation of filamentous microbes. In a first screen, the following culture media (1/5 dilution of the standard; 15 g of agar per liter) were used: 1) malt extract agar (MEA; Condalab; 2.69 g of the powder, 133 mL of ASW1 or 100 mL of ASW2 solutions and distilled water to 400 mL); 2) potato dextrose agar (PDA; Condalab; 3.12 g of the powder, 133 mL of ASW1 or 100 mL of ASW2 solutions and distilled water to 400 mL); 3) corn meal agar (CMA; Condalab; 1.36 g of the powder, 133 mL of ASW1 or 100 mL of ASW2 solutions and distilled water to 400 mL); 4) Lc medium (2g Arabic gum, 2 g olive oil, 0.2 g yeast extract, 0.4 g peptone,

2.42 g PIPES (1,4-Piperazinediethanesulfonic acid), 133 mL of ASW1 or 100 mL of ASW2 solutions and distilled water to 400 mL; pH adjusted to 7.5 with NaOH); and 5) Pc medium (3.6 g brain heart infusion, 9.2 g NaCl, 2.42 g PIPES, 133 mL of ASW1 or 100 mL of ASW2 solutions and distilled water to 400 mL; pH adjusted to 7.5 with NaOH) [25,27,28].

A minimal medium (MMM) supplemented with different carbon and nitrogen sources was also prepared by adding, per liter, 250 mL of ASW2 solution and 10 mL of a salts plus trace elements solution (25 mL of a trace elements solution, 50 g KH_2PO_4, 10 g $MgSO_4.7H_2O$, 5 g $CaCl_2{\cdot}2H_2O$ per liter) [15]. The trace elements solution (40x) was prepared by adding, per liter, 20 g monohydrated citric acid, 20 g $ZnSO_4.7H_2O$, 2.84 g $FeSO_4{\cdot}7H_2O$, 0.15 g $MnSO_4{\cdot}H_2O$, 1.04 g $CuSO_4{\cdot}5H_2O$, 0.2 g H_3BO_3, 0.15 g $(NH_4)_6Mo_7O_{24}{\cdot}4H_2O$ and 0.2 g biotin.

2.3. Phenotypic screening of the fungal isolates.

To ease the screening of isolates, we decided to use solid MMM. First, agar concentration had to be decreased as low as possible because it could be used by the isolates as a carbon source. Agar concentration was decreased from 1.5% [25] to 0.4-0.5%, which was the minimum agar concentration allowing solidification of the culture medium and clean point inoculation (Figure S1). Minimal medium (0.5% agar) without the addition of an extra carbon source was used as a negative control, while the addition of glucose (2 g/L) was used as a positive control of growth. The commercial algal polysaccharides alginate (Sigma-Aldrich; G/M, guluronic acid (G) versus mannuronic acid (M), ratio not provided by the supplier) or fucoidan (*Laminaria japonica*, Carbosynth; *Fucus vesiculosus*, Sigma-Aldrich; or *Undaria pinnatifida*, Sigma-Aldrich) were added at a concentration of 2 g/L (20 g/L stocks). The phenotypes in these culture

media were compared to those shown in minimal medium with the β-glucan polysaccharide laminarin (from *Thallus laminariae*; Carbosynth; ratio of β-1,3 and β-1,6 glycosidic linkages not determined by the supplier; also, at 2 g/L), which in general is more easily degraded by microorganisms [13]. Ammonium tartrate (9.2 g/100 mL; 100x) or sodium nitrate (4.25 g/100 mL; 100x) were added as the main nitrogen sources, to compare any possible effect of media acidification (ammonium) or alkalinization (nitrate) in the growth of fungal isolates, and also a hypothetic use of tartrate as a carbon source. Overall, we considered an isolate for further analysis when it showed greater radial growth rate on minimal medium supplemented with the polysaccharide than on minimal medium without an extra carbon source (negative control; only bacteriological agar). This phenotype had to be observed both when ammonium tartrate or sodium nitrate was used as the nitrogen source.

2.4. Extraction of genomic DNA, ITS amplification and Sanger sequencing.

Isolates were cultured in liquid minimal medium (28º C, 170 rpm) supplemented with ammonium tartrate and glucose as nitrogen and carbon sources. Incubation times varied depending on the growth rate of each isolate. Mycelia were filtered using Miracloth paper and lyophilized. Samples were processed with a Next Advance Bullet Blender homogenizer and genomic DNA fractions were extracted following the 1) phenol:chloroform:isoamylalcohol (25:24:1; Panreac AppliChem) method or, alternatively, 2) the guidelines of the NucleoSpin Plant II Mini kit (Macherey-Nagel), which uses hexadecyltrimethylammonium bromide (CTAB) in the lysis buffer [29]. The integrity of the samples was checked by agarose electrophoresis (0.8%).

Using genomic DNA samples as template, ITS regions or a fragment of the gene *rpb1*, which encodes the main subunit of the RNA polymerase II complex, were amplified

using oligonucleotide pairs ITS5 (GGAAGTAAAAGTCGTAACAAGG) and ITS4 (TCCTCCGCTTATTGATATGC), ITS4 and ITS1 (TCCGTAGGTGAACCTGCGG), and/or Rpb1-Up (GAATGCCCAGGTCATTTCGG) and Rpb1-Dw (CCAGCGATATCGTTGTCCATATA) [25,30,31]. The Kapa Taq DNA polymerase (Kapa Biosystems) was used for amplification (denaturation: 30 seconds at 95º C; annealing: 30 seconds at 54º C; elongation: 60 seconds at 72º C; 25 cycles). Amplification and specificity of the amplicons were checked by agarose electrophoresis (2%). Amplicons were purified using the Macherey-Nagel NucleoSpin gel and PCR clean-up kit and Sanger sequenced at Secugen S.L. (Madrid, Spain). The Sankey diagram was generated at SankeyMatic (https://sankeymatic.com/).

2.5. Genome sequencing and analysis.

Genomes of isolates M60 and M98 were initially sequenced using the Illumina MiSeq platform at the General Services of the University of the Basque Country (UPV/EHU), and later re-sequenced at the CNAG (https://www.cnag.crg.eu/), combining the Illumina NovaSeq platform and Oxford Nanopore Technologies GridION sequencing. Samples were quality-checked at the UPV/EHU and CNAG facilities before sequencing. See data availability for the two whole genome shotgun projects in section 9.

Galaxy (v22.05.1) was used to process genome-sequencing data [32]. The workflow *Itsas_Genomak* can be accessed in the following link: https://usegalaxy.org/u/oilier/h/itsasgenomak. Spades (versions v3.13.1) was used for hybrid genome assembly combining all Illumina and Nanopore sequencing files [33]. The provided assembly was modified to comply with JGI standards by removal of contaminants, organellar sequences, and small unsupported scaffolds, if present. The JGI Fungal Annotation pipeline [34,35] was used to predict genes, provide functional

annotations and carry out KOG (EuKaryotic Orthologous Groups) analyses, which were compared with those of closely related species. The trees in the heatmaps showing KOG analyses were generated, using the IDs of the species analyzed, with the common tree function at the NCBI taxonomy browser, and were formatted using iTOL [36]. A mitochondrial scaffold in each dataset was extracted from the main assembly and is presented separately as the mitochondrial assembly. Both datasets are accessible at https://mycocosm.jgi.doe.gov/Marma1 for *M. marquandii* and https://mycocosm.jgi.doe.gov/Albya1 for *A. yamanashiensis* [34].

BUSCO (Benchmarking Universal Single-Copy Orthologs; v5.2.2; hypocreales_odb10 dataset) was used for the assessment of the completeness of genome assemblies [37,38]. ANI (average nucleotide identity) and AAI (average amino acid identity) for species proximity were carried out at enveomics [39] and with AAI-profiler [40] (both websites were accessed in May 2023 and December 2024). The genomes and proteomes used in ANI and AAI analyses were downloaded from the NCBI database (Table S1). CAZyme analyses were carried out at the dbCAN3 website (accessed in December 2024 [41,42]) and results were compared to those provided by MycoCosm, which were obtained after a semi-manual curation of protein filtered model sequences by the CAZy team [43]. The dbCAN3 website uses three tools for automated CAZyme annotation: HMMER for annotated CAZyme domain boundaries, DIAMOND for fast blast hits in the CAZy database, and HMMER for dbCAN-sub, a database of carbohydrate active enzyme subfamilies for substrate annotation. Following the recommendation of the dbCAN3 tool, we excluded from our analyses all the CAZymes predicted only by one of those three tools (1674 and 1403 in the case of M60 and M98, respectively). dbCAN3 also predicted the presence of signal peptides in CAZymes using SignalP. To identify

sulfatases, the Sulfatlas website (v2.3.1) was used [44]. The fungal version of AntiSMASH 7.0 was used for prediction of secondary metabolite gene clusters [45].

2.6. Phenotypic characterization of isolates M60 and M98.

For microscopy analyses, isolates M60 (*Marquandomyces marquandii*) and M98 (*Albophoma yamanashiensis*) were inoculated in liquid MMM supplemented with glucose and ammonium tartrate and cultured at 170 rpm and 28º C. Culture times varied depending on the growth rate of each isolate. Samples of each culture were analyzed using a Nikon Eclipse E100 microscope equipped with an Imaging Source DFK23UP031 camera. Alternatively, a Nikon Eclipse Ci manual upright microscope was used, which included 40× and 100× (oil) Nikon CFI Plan Fluor lenses and a Teledyne Photometrics Moment camera. ImageJ (https://imagej.nih.gov/ij/) (US. National Institutes of Health, Bethesda, MA, USA) was used to process phase contrast images.

For characterization on solid MMM medium, glucose, mannose, fucose or fucoidans from *F. vesiculosus* or *U. pinnatifida* (see above) were used as main carbon sources at a concentration of 2 g/L (20 g/L stocks). Tolerance to salt stress was tested by adding increasing concentrations (0.2, 0.5, 1.0, 2.0 and 3 M) of NaCl to the culture medium. Optimal growth temperatures were determined by testing growth of both isolates at 25, 30, 35 and 37º C. Pigment secretion by *M. marquandii* was assessed and co-cultures of fungal strains were carried out on PDA, MEA, *Aspergillus* minimal (AMM) [46] or Yeast extract, Peptone and Dextrose (YPD) media.

For characterization of pigment production, coloring of media in *M. marquandii* cultures was followed by measuring optical density. Briefly, 10^6 spores/mL were inoculated in Erlenmeyer flasks filled with 250 mL of potato dextrose broth (PDB),

malt extract broth (MEB) or liquid AMM (glucose and ammonium tartrate were used in the latter case as carbon and nitrogen sources, respectively). Three flasks were inoculated per culture medium. Spores were cultured at 25º C. Samples of 2 mL were taken every 24 hours and filtered using Minisart 0,2 µm pore filters (Sartorius). Optical density was measured at 380 nm (NanoDrop 2000c, Thermofisher Scientific), for 14 days.

2.6. Co-cultures of fungal isolates.

M. marquandii was co-cultured with other strains of our collection (M98 – *A. yamanashiensis*; M122 – *genus Acrostalagmus* according to ITS/*rpb1* sequencing data; and MFuc12 – *genus Gliomastix*) as well as with *Aspergillus nidulans* strain TN02A3 [47], on Petri dishes of 14 cm filled with MEA, PDA or AMM culture media. *M. marquandii* was point-inoculated first, and cultured at 25º C. After 96 hours for *A. yamanashiensis* isolate M98 and *Gliomastix* isolate MFuc-12, or 144 hours for *A. nidulans* strain TN02A3 or *Acrostalagmus* isolate M122, the second strain was point-inoculated at a distance of 2.5 cm.

2.7. RNA extraction and sequencing.

Spores of *A. yamanshiensis* were collected from MEA cultures (168 hours of incubation at 25 ºC in the dark) and added (10^6 spores/mL) to liquid MMM supplemented with ammonium tartrate and one of the following three carbon sources: 1) mannose, as control, 2) fucoidan from *Fucus vesiculosus* or 3) fucoidan from *Undaria pinnatifida*. Spores of *M. marquandii* (10^6 spores/mL) were also added to MEB and PDB media (malt extract and potato dextrose broth, respectively). The cultures of *M. marquandii* were incubated for 168 hours (MEB versus PDB) and those of *A. yamanshiensis* (mannose versus fucoidan) for 21 days, at 25º C in the dark (static cultures in 6-well

plates). Mycelia from each 6-well plate were collected in 50 mL polypropylene tubes (three replicates per strain and culture medium). Samples were then centrifuged for 15 minutes at 4º C and 4,000 rpm, filtered with Miracloth paper, freezed and homogenized in a mortar using liquid nitrogen, collected in 2 mL tubes and stored in liquid nitrogen until RNA extraction. RNA samples were obtained by using the NucleoSpin RNA Plant kit from Macherey-Nagel, following the protocol for RNA isolation from filamentous fungi and using RAP buffer for cell lysis. RNA samples were quality-checked by agarose electrophoresis (1.2%) and by measuring A260/A280 as well as A260/A230 ratios (NanoDrop 2000c, Thermofisher Scientific). Finally, samples were stored at -80º C.

Sequencing libraries were prepared with VAHTS Universal V10 RNA-seq Library preparation kit for Illumina (Vazyme). The kit converts the messenger RNA (mRNA) into dual-indexed libraries. mRNA was captured from total RNA using VAHTS mRNA Capture Beads 2.0 kit (Vazyme). Oligo(dT) magnetic beads purify and capture the mRNA molecules containing polyA tails. Input RNA was 100 ng of total RNA. The purified mRNA was fragmented and copied into first strand complimentary DNA (cDNA) by using reverse transcriptase and random primers. In a second strand cDNA synthesis step, dUTP replaced dTTP to achieve strand specificity. End-repair and d(A)-Tailing were combined with second strand cDNA synthesis step. The final step was ligation of adapters, using 1/10 dilutions of adapters. The resulting products were purified and size-selected for an insert size of 200-300 bp. The size-selected adapter-ligated fragments were amplified for sequencing on an Illumina system. The combination of both kits offered a polyA capture to selectively sequence mRNA, strand information on RNA transcripts, and unique dual (UD) indexing with unique

combination of premixed Index 1 (i7) and Index 2 (i5) adapters (VAHTS Maxi Unique Dual Index DNA Adapters Set 1).

All libraries had an average size of 280-400 bp, with a mean size of 350 bp. Most of the samples showed a 140 bp peak which corresponded to adapter dimers. In order to remove the adapter dimers, all samples were pooled. An equimolar lane mix was prepared, calculated from the LabChip GX Touch profiles in the range of 200-100 bp, and a second round of bead purification was performed on the lane mix. Then, lane mix was quantified using QuBit dsDNA HS DNA kit. Library sequencing was carried out in an Illumina NextSeq 550 system (MidOutput Flow-cell; 150 cycles; paired-end; 2 x 76 bp read length). FASTQ files were demultiplexed and split into samples specific files (one per direction) using "Generate Fastq" module from NextSeq 550 software. All data processing and analysis was done in the Illumina BaseSpace Sequence Hub, using Dragen toolkits. Quality control of raw fastq files was carried out with Dragen FastQC + MultiQC tool v3.9.5 toolkit. Adapter and quality trimming and sequence length filtering was carried out with Dragen fastq v1.3.1 toolkit (minimum read length of 50 bp). Dragen reference builder v4.3.6 toolkit was used to build custom reference genomes for *A. yamanshiensis* and *M. marquandii*, while Dragen RNA v4.3.7 toolkit was used for alignment and mapping against custom reference genomes, and for differential expression analyses. Principal component analysis (PCA) plots were also generated with ClustVis [48] and plots for GO enrichment analyses and correlation matrices with R Studio (v2024.09.1+394; clusterProfiler package). See data availability in section 9.

2.8. Crude protein extracts and mass-spectrometry analyses.

The same culture procedure as described in the previous section was followed for crude protein extraction from *A. yamanshiensis*. Samples (three replicates per carbon source: mannose or fucoidan from *F. vesiculosus* or from *U. pinnatifida*) were lyophilized overnight before protein extraction. Lyophilized samples were homogenized (Bullet Blender; Next Advance) and cultured in 1 mL of Drubin buffer [49] for 90 minutes at 4º C in a rotary shaker, before centrifugation at 14000 rpm and 4º C. Supernatants (crude protein extracts) were collected into new tubes. Aliquots of 100 µL per sample were preserved for protein quantification while the remaining extracts were stored at -80º C. Protein concentration was determined by measuring OD_{595nm} using Bradford reagent.

For in-solution tryptic digestion, proteins were first extracted by incubating for 30 minutes, at room temperature under agitation, the samples in a buffer containing 7 M urea, 2 M thiourea, and 4% CHAPS (3-[(3-Cholamidopropyl)dimethylammonio]-1-propanesulfonate hydrate). Digestion was carried out by following, with minor modifications, the FASP protocol described in [50]. Trypsin was added in 50 mM ammonium bicarbonate to a trypsin-to-protein ratio of 1:10, and the mixture was incubated overnight at 37º C. Peptides were dried out in an RVC 2-25 speedvac concentrator (Christ) and resuspended in 0.1% formic acid (FA). Peptides were desalted and resuspended in 0.1% FA using C18 stage tips (Millipore) prior to acquisition.

Proteomics analysis of the samples was carried out in a nano-liquid chromatography with electrospray ionization (nLC-ESI) equipment (Evosep One) coupled to trapped ion mobility/time of flight (TIMS/TOF) tandem mass spectrometer (timsTOF PRO, Bruker). Peptides from digested proteins were separated in a C18 nano-flow UPLC column (15 cm x 150 µm internal diameter, 1.9 µm particle size; EV1106, Evosep) using the Evosep 30SPD standardized method (44 minutes gradient). tims/TOF spectra

of the samples were acquired through data independent acquisition (DIA). DIA data was processed with DIA-NN software for protein identification and quantification using default parameters [51]. Searches were done against *Albophoma yamanashiensis* M98 database (downloaded from https://mycocosm.jgi.doe.gov/Albya1) in library-free mode. Carbamidomethylation of Cys residues was considered as fixed modification and Met oxidation as variable modification. Data was loaded onto Perseus platform [52] for data processing (log2 transformation, imputation) and statistical analysis (Student's t-test).

3. Results.

3.1. Sordariomycetes, Dothideomycetes and Eurotiomycetes dominate cultivable fungi in coastal marine sediments of the Basque Country

A total of 273 isolates were obtained from coastal sediment samples (six estuarine stations and one coastal marine station; Figure 2A), exhibiting multiple phenotypic features (examples shown in Figure 2B). The phenotypes of 235 isolates (80% of the collection) were characterized in four of the culture media used for isolation (PDA, MEA, Pc and Lc; Figure S2) to identify isolates showing the same or similar phenotypes. Our results suggest that multiple isolates corresponded to the same strains, or strains of the same species showing subtle phenotypic differences (colored squares in Figure S2).

Genomic DNA of a number of isolates (50; 18% of the collection) was extracted. The ITS (internal transcribed spacer) region and/or an internal region of the gene *rpb1* were amplified by PCR from each DNA sample and sequenced (Figure 2C). Sordariomycetes (22) and Eurotiomycetes (19) were the most represented classes in the cultivable mycobiota of estuarine sediments of the Basque Country, followed by Dothideomycetes (8). *Penicillium* (Eutoriomycetes) was clearly the dominant genus (13), followed by

Marquandomyces (4) and *Acremonium* (3) among Sordariomycetes and *Cladosporium* (2) and *Stagonospora* (2) among Dothideomycetes.

3.2. Potential pigment producers: Identification and phenotypic characterization of isolate M60 (*Marquandomyces marquandii*).

After a preliminary characterization of the isolates, we initially directed our search towards the identification of pigment producers (see examples in Figure 3A). Among pigment producers, isolate M60 (estuary of river Artibai, winter 2021) developed purple colonies and stained MEA and mainly PDA media in yellow (Figure 3B-C), indicating the secretion of pigments. Sanger sequencing of the ITS region suggested that isolate M60 was *Marquandomyces marquandii* [53], with a nucleotide identity above 99.4% when compared with the best NCBI hits GU566261.1 and OM647857.1.

Microscopic analyses showed that M60 generated hyphal and developmental structures similar to those described for the species *M. marquandii* (Figure 3B) [53,54]. In liquid MMM and after 6 days of culture at 30º C and 180 rpm, we did not observe the formation of fully developed conidiophores but formation of side-branches in hyphae, each developing a single conidium [54]. The formation of these simplified asexual structures could be a consequence of carbon starvation, as occurs in the model fungus *Aspergillus nidulans* [55,56]. Radial growth of *M. marquandii* was bigger on MEA medium than on PDA or MMM medium (see the graph in Figure 3C). For example, after 16 days of culture at 25º C, the diameter of *M. marquandii* colonies was 4.60 ± 0.10 cm in MEA, 3.63 ± 0.15 cm in PDA and 2.83 ± 0.06 cm in MMM (n = 3 replicates in each culture medium). Growth was completely inhibited at temperatures equal or higher than 35º C (Figure 3D). We also followed coloring of growth media by measuring OD values at 380 nm for 14 days (three replicates per culture medium;

Figure 3E). Pigmentation of the medium increased steadily in PDB medium (see the inset corresponding to day 7) and exponentially after day 10 in AMM.

Finally, the contact zones between *M. marquandii* and other fungal strains were analyzed in co-culture experiments. Spore pigmentation and colony diameter of *A. nidulans* changed drastically in MEA or PDA media (yellowish green colonies with bigger diameters) compared to AMM, where colonies were smaller, and conidia developed their characteristic dark green color (Figure 3F). Besides, the way in which colonies of both species contacted each other varied from MEA to PDA and mainly to AMM, with larger exclusion zones in the latter case. We also tested the colony phenotypes at contact zones between *M. marquandii* and specific strains from our collection of isolates (isolates M98: *A. yamanashiensis*; M122: genus *Acrostalagmus*; MFuc12: genus *Gliomastix*). In general, exclusion zones were larger when isolates were cultured on PDA compared to MEA (second row in Figure 3G), and this observation correlated with a more intense yellow pigmentation of the culture medium around *M. marquandii* colonies (first row).

3.3. Potential fungal degraders of fucoidan: Identification and phenotypic characterization of isolate M98 (*Albophoma yamanashiensis*).

Three types of fucoidan were used in the phenotypic screening, since the monosaccharide content, linkage type, degree of sulfation and the position of sulfate groups vary significantly among them [18,57–59]. Initially, we found that most isolates were able to grow with fucoidan from *L. japonica* (Figure S3), but this result may be biased due to impurities in this carbon source (purity of this polysaccharide not detailed on the supplier´s website). In the case of fucoidan from *F. vesiculosus* or *U. pinnatifida* (purity above 95 %), radial growth of fungal isolates was significantly restricted

compared to the use of fucoidan from *L. japonica* (Figures S3 and S4). In addition, *radii* of colonies of the isolates of our collection were, in general, higher when fucoidan from *U. pinnatifida* was used compared to that of *F. vesiculosus* (Figure S4). Isolate M98, isolated from the estuary of Artibai river in winter 2021, showed bigger radial growth in MMM supplemented with fucoidan of *F. vesiculosus* than in the negative control (Figure 4A), both when am monium tartrate and sodium nitrate were used as the nitrogen source (Figure S5). The same phenotype was observed for isolate M127, isolated from a sample of Oria river collected in summer 2021 (Figure S5). M98 showed a characteristic phenotype, producing pycnidia when cultured on PDA or MEA culture media (Figure 4B-C) [60,61]. These phenotypic traits had been previously described by Kobayashi and colleagues for *A. yamanashiensis* [62]. Thus, isolate M98 was initially associated to this hypocrealean fungus. Radial growth of isolate M98 was bigger on MEA and PDA media compared to MMM (Figure 4D). After 15 days of culture at 25º C, diameter of *A. yamanashiensis* colonies was 4.67 ± 0.06 cm in MEA, 4.50 ± 0.00 cm in PDA and 3.87 ± 0.12 cm in MMM (n = 3 replicates in each culture medium). Growth of this isolate was severely decreased at 35º C compared to 25º or 30º C, and impaired at 37º C.

Sanger sequencing of the ITS region of isolate M98 indicated that this isolate was a species of the genus *Tolypocladium*, with a nucleotide identity above 99.8% in all cases (best hit NCBI accession number: AB457003.1). Alternatively, it may be identified as *Albophoma yamanashiensis*, with a nucleotide identity above 99.6% in all cases (best hit NCBI accession number: OW983802.1). Sequencing of *rpb1* suggested that it belonged to the genus *Tolypocladium* (nucleotide identity above 96.1%; best hit NCBI accession number: KF747240.1).

3.4. Genome sequencing and features of isolates M60 and M98.

Isolate M60 was selected for genome sequencing due to its ability to stain the culture medium in yellow. Isolate M98 was selected due to its characteristic phenotype, including the apparent capability of growing on medium supplemented with fucoidan.

The size of the quality filtered assemblies of isolates M60 and M98 was 43.61 Mb and 31.18 Mb, respectively (see general data in Table 1; see their entry at Mycocosm: https://mycocosm.jgi.doe.gov/Marma1 and https://mycocosm.jgi.doe.gov/Albya1). The number of *contigs* longer than 2,000 bp were 97 and 38 for the two isolates. The largest *contigs* of M60 and M98 assemblies were of 5.62 and 4.47 Mbp, respectively. Annotation of each assembly led to the prediction of 12,408 and 10,216 proteins for isolates M60 and M98, respectively (Table 1). Completeness estimates were 97.2% for both assemblies and single-copy BUSCO shares ranged between 96.2% for M60 and 96.4% for M98, indicating high completeness and low redundancy of processed genomic data based on universal single-copy orthologs of Hypocreales. Average nucleotide identity (ANI) values were calculated among isolates and different species of the order Hypocreales (Figure 5A), including a reference genome of *A. yamanashiensis* (Genbank accession number BCKH01000001.1; Table S1). The highest ANI values for isolate M60 were obtained with species of *Metarhizium* and *Pochonia* (Figure 5A), which aligns with the results described by [53]. For isolate M98, the percent identity with the reference genome of *A. yamanashiensis* was 99%.

KOG (euKaryotic Orthologous Groups) analysis for isolates M60 and M98 were compared to those of Hypocreales species at MycoCosm. Since *Marquandomyces marquandii* was initially known as *Paecilomyces marquandii* [53,54], two species of the *genus Paecilomyces* (class: Eurotiomycetes; order: Eurotiales), *P. variotii* and *P. niveus*,

were included in the comparison (Figure S6A). *M. marquandii* M60 showed the second highest content in KOG group Q (Secondary metabolites biosynthesis, transport and catabolism), while in the case of KOG groups G (Carbohydrate transport and metabolism) and M (Cell wall/membrane/envelope biogenesis) it was the first and third most abundant, respectively. In the case of KOG groups M and G, *A. yamanashiensis* was in both cases the sixth genome with the highest content. These values were in line with the total KOG counts for each species (second highest for *M. marquandii* and eight for *A. yamanashiensis*).

3.5. Genomic analysis of the potential for secondary metabolite production of *M. marquandii* M60 and *A. yamanashiensis* M98.

Among the 21 genomes analysed in the KOG analysis, that of *M. marquandii* isolate M60 had a high number of backbone enzymes of secondary metabolite gene clusters (57, fourth genome in the ranking), while *A. yamanshiensis* M98 had 44 (seventh in the ranking; Figure S6B). However, the latter genome was particularly enriched in genes encoding hybrid NRPS (non-ribosomal peptide synthetase)-PKS (polyketide synthase) enzymes and NRPS enzymes, being at the second position of the ranking for both gene categories. In contrast, *M. marquandii* M60 had the second highest number of NRPS-like enzymes.

Considering the potential of *M. marquandii* for secondary metabolite and pigment production, and that of *A. yamanashiensis* as a producer of terpendole E, an inhibitor of enzymes involved in cholesterol metabolism [63], we annotated secondary metabolite gene clusters in the genomes of isolates M60 and M98 [45] by using antiSMASH (Figure 5B). We further compared this analysis with that at the MycoCosm website. The analysis confirmed previously observed general trends and suggested that the genomes

of *A. yamanashiensis* and mainly *M. marquandii* encoded a high number of fungal RiPP-like compounds [64]. RiPPs are synthesized from precursor peptides in which a leader peptide is identified and removed by modifying enzymes, leaving a core peptide on which post-translational modifications occur [65].

AntiSMASH predicted the presence of 84 secondary metabolite gene clusters in the genome of isolate M60 (Figure S7), including 11 secondary metabolite gene clusters with similarity equal to or higher than 50%. Similarity of 100% was assigned to clusters c2.6 (ε-Poly-L-lysine, a non-ribosomal peptide), c3.3 (choline; non-ribosomal peptide), c9.1 (FR901512; polyketide), c15.1 (1,3,5,8-tetrahydroxynaphthalene; polyketide), and c16.1 (dymethylcoprogen, non-ribosomal peptide), while similarity percentages ≥80% was assigned to the clusters for the synthesis of sorbicillins and hypothemycin polyketides, both molecules with therapeutic activity as antifungals, antiparasitic and antitumor [66–68].

In the case of the *A. yamanashiensis* isolate (M98), antiSMASH predicted the presence of 59 secondary metabolite gene clusters, including 7 with similarity higher than 70% compared to those known to synthesize the compounds as indicated in Figure S8. A similarity of 100% was assigned to clusters c2.2 (terpendole E; terpene) [63], c5.2 (choline; non-ribosomal peptide), and c7.3 (polyketide + non-ribosomal peptide), the latter being necessary for the synthesis of tolypyridone C, a phenylpyridine with antibacterial and antifungal activity [69].

3.6. CAZyme repertoires of *M. marquandii* M60 and *A. yamanashiensis* M98.

The predicted CAZyme (carbohydrate-active enzymes) repertoires of isolates *M. marquandii* M60 and *A. yamanashiensis* M98 were analyzed to assess their potential to degrade complex algal polysaccharides. A total of 656 and 403 proteins with CAZy

domains were predicted for M60 and M98, respectively, by the CAZy annotation pipeline and available in MycoCosm (Figure 5C). Similarly, 610 (M60) and 365 (M98) CAZymes were predicted, respectively, by at least two of the tools used by dbCAN3 (Tables S2, S3). A total of 213 (34.9%; M60) and 143 (39.2%; M98) of the CAZymes predicted by dbCAN3 were also predicted to include a signal peptide in their sequence and would therefore represent the set of potentially secreted CAZymes of those isolates.

In the case of isolate M60, 101 proteins were predicted to include AA domains (auxiliary activity family protein) from CAZy classification, 47 proteins with CBM domains (carbohydrate-binding module), 23 with CE domains (carbohydrate esterase), 339 with GH domains (glycoside hydrolase), 123 with GT (glycosyl transferase) and 9 with PL (polysaccharide lyase) domains. For M98, dbCAN3 predicted a significantly lower number of GHs, 169, plus 53 AAs, 23 CBMs, 14 CEs and 121 GTs. Overall, the genome of *M. marquandii* M60 is predicted to encode the highest number of CAZymes among the species compared in this work. In most cases, this is probably associated with *M. marquandii* being the species with the highest number of predicted protein-coding genes. However, the genome of *Pochonia chlamydosporia* 170 is predicted to encode 14,204 proteins, compared to 12,408 in the case of *M. marquandii* M60 (1.14 times higher), while the number of predicted CAZymes in M60 is 649 compared to 538 in *P. chlamydosporia* (1.20 times higher in *M. marquandii* M60). *A. yamanshiensis* M98 is predicted to include a remarkable set of GT proteins, the highest number among the sequenced species of the Ophiocordycipitaceae family analyzed in Figure 5D. However, no PLs were identified, as occurs with sequenced genomes from the Clavicipitaceae family species *Claviceps purpurea* and *Ustilaginoidea virens* and the Ophiocordycipitaceae family species *Drechmeria coniospora* analyzed in this work.

Due to the ability of *A. yamanashiensis* isolate M98 to grow on medium supplemented with the recalcitrant polysaccharide fucoidan, we focused on the analysis of the CAZymes and sulfatases potentially involved in the degradation of this algal polysaccharide [18,70]. A limited number of proteins were found in M98, including one fucosidase of family GH29 and one of family GH95 (brown squares in Figure 5D). For comparison, 2 and 6 were predicted, respectively, in the case of *M. marquandii* isolate M60, plus 1 additional fucosidase of the GH141 family. Additionally, galactosidases and galacturonidases of GH36 (1) and GH28 (1) families were found in M98 (8 and 7, respectively, in the case of *M. marquandii* isolate M60).

Finally, SulfAtlas predicted that the genome of isolate M98 included genes encoding 7 sulfatases, of families S1_6 (2), S1_11 (1), S1_12 (1), S2 (1) and S3 (2). On the other hand, the genome of isolate M60 encoded 6 sulfatases, of families S1_4 (3), S1_8 (1) and S3 (2). Overall, the repertoire of predicted fucoidan-degrading enzymes and sulfatases in the fungal isolates characterized here is far more limited than the one described in the literature for fucoidan-degrading marine bacteria [18].

3.7. Comparison of the transcriptional patterns of *M. marquandii* M60 cultured on PDB versus MEB media: the sorbicillin gene cluster is strongly deregulated.

To determine the set of activities induced in *M. marquandii* for the secretion of the yellow metabolite, we compared the transcriptomic response of mycelia cultured on PDB versus MEB culture media. Samples were collected, based on the graph in Figure 3E, after 7 days of static culture at 25º C in the dark. Both replicates of each sample grouped together, with high correlation values (Figure 6A-B). Reads were detected for 8,661 genes, 69.8% of the 12,408 genes annotated in the genome of *M. marquandii* M60. A total of 2,550 differentially expressed genes were identified (adjusted $p < 0.05$);

1,075 were significantly upregulated in PDB medium compared to MEB while 1,475 were downregulated (Figure 6C; Table S4). The heatmap in Figure 6D shows the correlation in the replicates for Top100 up- and downregulated genes. Gene enrichment and functional analysis of significantly deregulated genes and the proteins encoded by the Top20 up-/downregulated genes showed that processes such as transport, transcriptional regulation or oxidation-reduction processes were among the most significantly deregulated molecular functions (Figure 6E-F). Furthermore, we observed the presence of secondary metabolite gene cluster genes among the Top20 deregulated genes.

We compared the list of significantly deregulated genes (adjusted $p < 0.05$) with that predicted by antiSMASH for *M. marquandii* M60 (Figure 5C), which included 1,240 genes in 84 predicted clusters (an average of 15 ± 7 genes per cluster; 32 genes in the longest cluster, while the shortest one is predicted to be composed of 3 genes). We focused on long (> 10 genes) secondary metabolite gene clusters with at least 35% of those genes being significantly deregulated in PDB medium compared to MEB (purple squares in Figure 6G). Clusters c1.3 (0.58; 12 genes) and mainly c6.5 (0.69; 16 genes) were those with the highest ratio of significantly deregulated genes versus genes in that cluster (Figure 6G-H). According to antiSMASH, cluster c1.3 showed low similarity (20%) compared to the imizoquin gene cluster from *Aspergillus flavus* NRRL3357 [71]. Imizoquins are a family of tripeptide-derived alkaloids that are produced via a nonribosomal peptide synthetase-derived tripeptide and have a protective role against oxidative stress during *A. flavus* germination. Cluster c1.3 was downregulated, with the gene encoding the backbone enzyme being the Top6 among downregulated genes.

Cluster c6.5 was annotated by antiSMASH as the sorbicillinoid gene cluster of *M. marquandii* (87% of similarity compared to the sorbicillin cluster of *Acremonium chrysogenum* ATCC 11550; [68]). The characteristic yellow pigment of *M. marquandii* has been described as a nitrogen-containing sorbicillinoid (see Discussion) [72]. Although two genes within cluster c6.5 of *M. marquandii* M60, encoding an MFS transporter and an acetylglutamate kinase, respectively, are slightly upregulated, most genes are downregulated, with the two PKS-encoding genes of the cluster being, respectively, the Top73 and Top53, and a third gene the Top18 of downregulated genes (Figure 6H).

3.8. Transcriptional and protein profiles of isolate M98 in response to fucoidan.

To identify the set of *A. yamanashiensis* M98 activities potentially involved in the processing of fucoidan from *F. vesiculosus* or *U. pinnatifida*, we compared its transcriptomics and proteomics responses to those in minimal medium supplemented with mannose, as a non-sulfated control monosaccharide that is present in some types of fucoidan. Mannose residues in these two types of fucoidan are less than 2% of the relative abundance of monnosaccharides [18]. Samples of *A. yamanashiensis* M98 were collected after 21 days of static culture at 25º C in the dark. The three replicates per condition grouped together, as can be seen in the PCA and correlation plots (Figure 7A-B). The following three comparisons were carried out: 1) genes differentially expressed in medium with fucoidan from *F. vesiculosus* versus mannose (FV_Vs_Mann), 2) genes differentially expressed in medium with fucoidan from *U. pinnatifida* versus mannose (UP_Vs_Mann), and 3) genes differentially expressed in medium with fucoidan from *U. pinnatifida* versus medium with fucoidan from *F. vesiculosus* (UP_Vs_FV). RNA-seq reads for more than 75% (75.3 to 77.1%) of the 10,216 genes annotated in the genome

of *A. yamanashiensis* M98 were detected in all comparisons. A total of 2,476 genes were differentially expressed (adjusted $p < 0.05$) in the first comparison (1,137 upregulated and 1,339 downregulated in FV_Vs_Mann); 2,480 in the second comparison (1,099 up- and 1,381 downregulated in UP_Vs_Mann); and 2,801 in the third one (1,353 up- and 1,448 downregulated in UP_Vs_FV; Figure 7C; Tables S5-S7). Figure 7D (colored squares) highlight the presence of genes up- or downregulated only in medium with fucoidan from *F. vesiculosus*, only in fucoidan from *U. pinnatifida* or in both cases, suggesting that the transcriptional responses to the two types of fucoidan overlap partially, but there are also specificities in each response pattern (Figure 7E). This pattern can also be seen in the Top20 up- and downregulated genes (Figure 8) and, overall, probably reflects the structural and compositional similarities and divergences of both types of fucoidan [18] (see Discussion). Common to both comparisons (FV_Vs_Mann and UP_Vs_Mann) were 609 upregulated (53.6 and 55.4%, respectively) and 842 downregulated (62.9 and 61.0%, respectively) genes, while 528 (46.4%) and 497 (37.1%) genes were specifically up- and downregulated in the FV_Vs_Mann response, and 490 (44.6%) and 539 (39.0%) genes were specifically up- and downregulated in the UP_Vs_Mann response.

The transcriptomics analysis was complemented with a proteomics analysis of crude protein extracts corresponding to samples collected under the same culture conditions. The three replicates per condition grouped together, as can be seen in the PCA and correlation plots (Figure 9A-B). The Heatmap in Figure 9C includes proteins with statistically significant changes ($p < 0.05$; Top300 of each comparison) in their levels in FV_Vs_Mann and UP_Vs_Mann comparisons (see also Table S8 with all proteomics data). It supports the trends in expression shown in the transcriptomics analysis in Figure 7D, strongly suggesting that *A. yamanashiensis* modulates, at least partially, the

response depending on the type of fucoidan. Among the Top20 up- and downregulated proteins in FV_Vs_Mann and UP_Vs_Mann responses, the overlap was of 45.0% (up) and 15.0% (down), respectively (Figure 9D, top; see also Figure 10), while in the case of proteins with FV/Mann or UP/Mann ratios above 10 (up) and below 0.1 (down), the overlap was of 29%/43.9% and 29.2%/30.9%, respectively. We also compared the lists of differentially expressed genes and proteins ($p < 0.05$; Figure 9E for induced proteins; Figure S9 for proteins with lower levels). These lists matched partially, with a 23.3%/15.6% overlap in the case of the FV_Vs_Mann comparison, and 25.0%/18.7% overlap in the case of the UP_Vs_Mann comparison.

We searched for CAZyme and sulfatases (and the corresponding genes) that were up- or downregulated at the protein level in the presence of fucoidan. In the FV_Vs_Mann comparison, one of the two S1_6 sulfatases (annotated as N-acetyl-D-glucosamine-6-sulfate 6-O-sulfohydrolase) of *A. yamanashiensis* was the Top2 protein with higher levels, with an FV/Mann ratio of 139.4 (Figure 9E and 10). Considering that sulfatases must be activated by sulfatase-modifying factors, we searched for genes encoding proteins with this domain (IPR005532) in the genome of *A. yamanshiensis*. One of them, mRNA_6814, was significantly upregulated in both FV_Vs_Mann (log2FC: 2.51) and UP_Vs_Mann (log2FC: 1.77) comparisons (statistically significant increase in protein levels only in the UP_Vs_Mann comparison). Furthermore, a protein annotated as a fucose-specific lectin was the Top6 (FV/Mann ratio of 71.1), a thiosulfate uptake-transporter was the Top38 (FV/Mann: 20.0), a sulfatase of family S3 ((R)-specific secondary-alkylsulfate sulfohydrolase) was the Top59 (FV/Mann: 15.6), and a glycosyl hydrolase of the GH72 family (β-1,3-glucanosyltransglucosidase) was the Top73 (FV/Mann: 13.6) protein (FV/Mann: 10.1) (indicated with asterisks in Figure 9E; see also Table S8). In the transcriptomics analysis, CAZyme-encoding genes with log2FC

values higher than 3 (asterisks in Figure 9E) were predicted to belong to families GH76 (log2FC: 6.4; mannan endo-1,6-α-mannosidase), AA1 (3.7); CE3 (3.6; acetylesterase), GT32 (3.6; GDP-Man: α-1,3-mannosyltransferase), and GH55_2 (3.1; glucan 1,3-β-glucosidase).

In the UP_Vs_Mann comparison, two GH38s (mannosyl-oligosaccharide exo-α-1,2-mannosidase or mannosyl-oligosaccharide endo-α-1,P-mannosidase) were the Top1 and Top10 proteins, with UP/Mann ratios of 136.0 and 60.8, respectively. The Top19 protein (UP/Mann ratio of 26.8; log2FC of 5.9) was annotated by Sulfatlas as a S1_11 protein (exo-N-acetyl-D-glucosamine-6-sulfate 6-O-sulfohydrolase; Heparin/Heparan 6-O-sulfate sulfatase). In addition, Top21 and Top32 proteins were annotated as MFS-type L-fucose permeases (UP/Mann: 26.9 and 16.8, respectively), the Top34 as a protein containing a CBM67 domain (15.9; α-L-rhamnosidase), the Top37 as a protein of the GH27 family (15.1; α-galactosidase; galactomannan exo-α-1,6-galactosidase) and the Top47 as a GH72 (12.2; β-1,3-glucanosyltransglucosidase; GPI-anchored proteins that remodel β-1,3-glucans of the fungal cell-wall). The Top61 protein is the same S1_6 sulfatase that was the Top1 protein in the FV/Mann comparison (10.4; N-acetyl-D-glucosamine-6-sulfate 6-O-sulfohydrolase). Finally, the Top63 protein was annotated as a GH64 (10.3; glucan endo-β-1,3-glucosidase) and the Top64 as a GH5_27 protein (10.3; endoglycosylceramidase).

In the transcriptomics analysis, a gene annotated as encoding a sulfatase of the S3 family (log2FC: 3.5; (R)-specific secondary-alkylsulfatase, type III), a GH20 family protein-encoding gene (log2FC: 4.1; β-N-acetylhexosaminidase), the same GH76-encoding gene as in the FV_Vs_Mann comparison (log2FC: 5.9; mannan endo-1,6-α-mannosidase), a gene encoding a GT2-family protein (3.9; GDP-Man α-

mannosyltransferase; α-1,4-L- or α-1,6-L-fucosyltransferase), the same GT32-encoding gene as in the FV_Vs_Mann comparison (4.0; GDP-Man: α-1,3-mannosyltransferase), a gene encoding a protein with a CBM32 domain (5.0; galactose oxidase), and a gene encoding a protein with an AA1 domains (5.0) were upregulated.

Overall, results from our proteomic and transcriptomic analyses for *A. yamanshiensis* strongly suggest that this fungus senses the presence of sulfated carbohydrates and activates a response mechanism (see Discussion).

4. Discussion.

The application of the *dilution-to-extinction* method [11] in estuarine sediment samples enabled the isolation of a large diversity of filamentous fungi showing a variety of growth patterns. Our results suggest that cultivable fungi from the studied estuaries are mainly represented by Eurotiomycetes and Sordariomycetes species. This agrees with previous culture-based studies where marine fungi seemed to be dominated by Eurotiomycetes (*e.g.*, *Aspergillus* and *Penicillium*), Sordariomycetes (*e.g.*, *Fusarium*, *Trichoderma*, *Marquandomyces*) and Dothideomycetes (*e.g.*, *Cladosporium* and *Ulocladium*) (see references within [7]). Nevertheless, the extreme differences in growth rates among marine fungal species in culture [11] may be biasing the real composition of fungi in the samples, as typically found for bacteria (*i.e.*, the great plate-count anomaly; [73]). Additional efforts in isolation and culturing of slow-growing fungi and the direct identification of fungal taxa by metabarcoding (see, for example, [10,74,75]) will contribute to the identification of previously undescribed species, some of them potentially harboring biotechnological potential.

The repertoire of secondary metabolism backbone enzymes in fungi is composed mainly of PKS, NRPS, dimethylallyltransferases (DMATs), and terpene synthases [76],

and the number of biosynthetic gene clusters per genome varies dramatically across species [76,77]. Here, we have focused on the description and comparison of specific genomic features of two species that were previously described phenotypically [53,54,62] but not at the genomic level. Interestingly, in both cases, the strains characterized phenotypically were originally isolated from terrestrial environments. On the one hand, *M. marquandii* has been reported to grow on mushrooms and soil, and their distribution covered Brazil, Netherlands, Russia, UK and USA [53]. On the other hand, *A. yamanshiensis* was isolated from a forest soil in Japan [62]. The isolation of strains of both species in sediment samples of Basque estuaries suggests that they are ubiquitously distributed and have adapted also to estuarine environments. While both isolates, M60 (*M. marquandii*) and M98 (*A. yamanashiensis*), correspond to species of the order of Hypocreales, the number of backbone enzyme-coding genes and secondary metabolite gene clusters is clearly higher in isolate M60 than in the genome of isolate M98, in correlation with the size of their genomes. However, the genome of isolate M98 is enriched in genes encoding specific backbone enzymes, such as hybrid NRPS-PKSs, compared to other Hypocreales species and includes gene clusters predictably involved in the synthesis of secondary metabolites of potential interest for biotechnology, such as Terpendole E, which acts as an acyl-CoA:cholesterol acyltransferase inhibitor [63] or as a kinesin Eg5 inhibitor [78].

There was a genome sequence of *M. marquandii* (synonims *Metarhizium marquandii* and *Paecilomyces marquandii*) available (Biosample: SAMN41475035), but the genome of this species had not been previously described in the literature. This fungus is able to produce a yellow pigment, which synthesis and secretion clearly depended on the composition of the culture medium (Figure 3A), as previously shown [53]. Using a *M. marquandii* strain isolated from a marine sediment sample collected in

Argentina, Cabrera *et al*. described that the yellow pigment is a nitrogen-containing sorbicillinoid, sorbicillinoid urea, a Diels-Alder product of sorbicillinol [72,79]. In general, sorbicillinoids represent an important family of hexaketide compounds produced by terrestrial and marine fungi, including species of *Marquandomyces*/*Paecilomyces*, and have a variety of biological activities of interest in biotechnology including cytotoxic, antioxidant, anti-inflammatory, antiviral and antimicrobial activity [80,81]. Due to their biotechnological potential, recent studies have tried to develop fungal systems for sorbicillinoid hyperproduction [82]. Remarkably, we found that isolates closely related to M60, such as M43-45, affiliated with *Marquandomyces marquandii*, showed similar but not identical phenotypes. In the case of isolate M45, we have not observed the production of the characteristic yellow metabolite secreted by M60. Comparative genomic analysis of these strains, or mutagenesis screenings, could contribute to the identification of point substitutions or insertions/deletions causing an inhibition of the synthesis of the mentioned yellow pigment.

The gene cluster c6.5 in the genome of M60 is predictably involved in sorbicillin biosynthesis, as it shows high identity with the sorbicillin gene cluster of *Acremonium chrysogenum* (Figure 6H) [68]. In *Penicillium chrysogenum*, the sorbicillin biosynthesis gene cluster includes two PKS-encoding genes, *sorA* and *sorB*, and two transcription factor-coding genes, *sorR1* and *sorR2* (SorR1 acts as an activator, while SorR2 controls the expression of *sorR1*) [83]. Sorbicillin clusters have been described in additional fungal species, such as *Trichoderma reesei* [84]. Here, cluster c6.5 included genes encoding the two PKSs and the two transcription factors, and probably incorporates a gene encoding a third transcription factor (all three of the Zn_2Cys_6 family), adding a new layer of complexity to its regulation (Figure 6H). Our RNA-seq results suggest a

general downregulation of the sorbicillinoid cluster of *M. marquandii* after 7 days of static culture at 25º C in PDB compared to malt extract broth, with the exception of the genes encoding an MFS transporter and a kinase. Figure 3E shows that at this time point the intensity of the yellow coloration of the PDB medium is still increasing. With these results, it is tempting to suggest that, in PDB medium, the concentration of the final product of the sorbicillinoid biosynthetic pathway of *M. marquanddi* is lower compared to the MEB medium and/or that the yellow pigment is not the final product of the biosynthetic pathway. However, the pigment would be accumulated in the PDB medium due to higher expression and protein levels of the transporter and a higher export capacity. Metabolomics analyses are needed to inform of the metabolic profile of organic extracts from *M. marquandii* grown on PDB or MEB media.

In the case of M98, this isolate was selected for genome analysis because the genome of *A. yamanshiensis* had not been described in detail and due to its apparent growth on fucoidan. This name refers to polysaccharides containing high percentages of L-fucose and sulfate ester groups, and are mainly derived from brown seaweed [70]. Fucoidans are highly diverse polysaccharides [18]. They can be grouped into homofucans (α-1,3- or alternating α-1,3-/α-1,4-linked fucose backbone with sulfate esters on positions *O*-2, *O*-3 or *O*-4) or hetero-polysaccharides with a non-fucose backbone consisting of mannose, galactose or glucuronic acid with side-branches of sulfated fucose [18]. These two types of main backbones can include additional modifications, increasing the diversity of fucoidans. The structure and composition of the two types of fucoidan used in this work were described previously by Sichert and colleagues [18]. That work also described that for fucoidan degradation bacteria use glycosyl hydrolases belonging to families GH29 (exo α-1,2-L-fucosidase), GH95 (α-L-fucosidase/α-L-galactosidase), GH141 (α-L-fucosidase/xylanase) and GH107 (endo-α-L-fucanase). The same authors

also described that families GH36 (α-galactosidase, α-N-acetylgalactosaminidase), GH116 (β-glucosidase, β-xylosidase, acid β-glucosidase/β-glucosylceramidase, β-N-acetylglucosaminidase), and GH117 (β-D-galactofuranosidase) may be fucoidanases with a yet unknown function, and that families GH28 (polygalacturonase) and GH155 (glucuronidase; family removed from the CAZYme database; [85]) remove acetate, galacturonic acid and glucuronic acid, which are present in specific types of fucoidan. This set of GHs include both exo and endo activities, degrading internal and external (usually from the non-reducing end) glycosidic bonds. Regarding the analysis of sulfatases, subfamilies S1_15, S1_16, S1_17 and S1_25 have been reported as necessary for fucoidan degradation or enriched in fucoidan-degrading marine bacterial proteomes [18]. A recent work has shown that commercial fucoidan from *U. pinnatifida* (Sigma F8315) causes an upregulation of the same CAZyme and sulfatase families in Planctomycetota bacteria [86]. Considering that the same product reference was used in the present work and that the genome of *A. yamanshiensis* encodes a completely different repertoire of CAZyme and sulfatases, as seem to do fungi in general, the identification of the enzymes induced in response to fucoidans with different structures is interesting for biotechnology.

As a result, we have identified several induced sulfatases, such as those predictably belonging to families S1_6, S1_11 and S1_12. The genome of *M. marquandii* is not predicted to encode these sulfatase activities. For example, fucoidan from *U. pinnatifida* causes strong upregulation and higher protein levels of an S1_11 sulfatase. The Sulfatlas website associates this family with desulfation of polysaccharides such as heparin or chondroitin and glycoproteins such as mucins [87]. Thus, it will be interesting to determine in the future if fungal S1_11 sulfatases can act on sulfate groups of specific types of fucoidan. Furthermore, and considering that according to the

Sulfatlas database only two experimentally determined structures of S1_11 sulfatases are available in the Protein Data Bank database (each with or without a ligand), both of them belonging to gut bacteria [88,89], this protein from *A. yamanshiensis* would constitute the first experimentally determined structure of a fungal S1_11 sulfatase.

In combination with sulfatases, the apparent induction of a sulfatase-modifying factor-coding gene, fucose-specific lectins, and L-fucose permeases strongly suggest that *A. yamanshiensis* senses and responds to the presence of carbohydrates composed of sulfated L-fucose. Although the set of upregulated GHs identified in our transcriptomics and proteomics analyses includes an exo-1,2-α-L-fucosidase (GH95), in general the CAZyme families point to processing of mannans and glucans. These two polysaccharides are components of the fungal cell wall, and their relative abundance varies depending on the clade. For example, mannans are more abundant and essential in the outer cell wall of *Candida*, while they are much less abundant in *Aspergillus* [90,91]. Although the composition of the cell wall of *A. yamanshiensis* has not been determined, the induction of those activities points to a model in which this fungus responds by remodeling its cell wall structure, maybe to obtain a more easily metabolizable carbon source. Future experiments will have to determine whether these enzymes have hitherto undescribed activities on fucoidan or are employed by fungi to remove mannose from fucoidan, although the percentage of this monosaccharide is lower than 2% in the types of fucoidan used in this work [18]. However, it can be concluded from the analysis of fungal genomes that if fungi are able to process recalcitrant marine polysaccharides such as fucoidan, they follow completely different mechanisms compared to bacteria.

5. Acknowledgements.

We want to thank all groups and members of the EMOTION consortium, funded by the Basque Government (see Funding), for their support. The authors acknowledge technical and human support provided by the General Research Services (SGIker) of the UPV/EHU (ERDF and ESF funding), especially Dr. I. Bernales and Dr. I. Miguel, and the CNAG-CRG for assistance with genome and transcriptome sequencing projects.

6. Funding.

Work at O.E´s and L.A-S labs was funded by the Basque Government, projects KK-2021/00034 and KK-2022/00107 (Elkartek Call). O.E´s and R.L´s labs also thank the Basque Government for grants IT1662-22 and IT1741-22, respectively, and AEI for grant PID2023-147050NB-I00 to R.L. Diputación Foral de Gipuzkoa granted O.E´s lab with grants DG23/07 and DG24/05. The work conducted by the U.S. Department of Energy Joint Genome Institute (https://ror.org/04xm1d337), a DOE Office of Science User Facility, is supported by the Office of Science of the U.S. Department of Energy under Contract No. DE-AC02-05CH11231. The funders had no role in study design, data collection and interpretation, or the decision to submit the work for publication.

8. Author contributions.

O.E. and L.A.-S. conceived the project. A.O., Z.A., C.P.-C, R.L., M.D., M.O., R.L. and O.E. performed the experiments. M.A. and F.E. carried out proteomics analyses. A.L. assembled the genomes of *M. marquandii* and *A. yamanshiensis*, and S.H. and I.V.G. provided and coordinated annotation resources. All authors analyzed the results. O.E. and Z.A. wrote the first version of the manuscript. All authors edited and improved the manuscript.

9. Availability of Data and Material.

The genome assemblies and annotations for *Marquandomyces marquandii* M60 and *Albophoma yamanshiensis* M98 are available from JGI MycoCosm (https://mycocosm.jgi.doe.gov/Marma1 and https://mycocosm.jgi.doe.gov/Albya1) and have also been deposited at DDBJ/ENA/GenBank under accessions **JAUIRS000000000** (BioProject **PRJNA990752**; BioSample **SAMN36274215**) and **JAUIRT000000000** (BioProject **PRJNA990765**; BioSample **SAMN36274349**), respectively. RNA-seq data for *M. marquandii* (MEB vs PDB media) were deposited under BioProject **PRJNA1233808** and BioSample **SAMN47279085** accession codes. RNA-seq data for *A. yamanashiensis* (mannose vs fucoidan) were deposited under BioProject **PRJNA1233821** and BioSample **SAMN47279930** accession codes.

10. Competing interest.

The authors declare no competing interests.

References.

[1] T. Niskanen, R. Lücking, A. Dahlberg, E. Gaya, L.M. Suz, V. Mikryukov, K. Liimatainen, I. Druzhinina, J.R.S. Westrip, G.M. Mueller, K. Martins-Cunha, P. Kirk, L. Tedersoo, A. Antonelli, Pushing the frontiers of biodiversity research: Unveiling the global diversity, distribution, and conservation of fungi, Annu. Rev. Environ. Resour. 48 (2023) 149–176. https://doi.org/10.1146/annurev-environ-112621-090937.

[2] J.W. Spatafora, M.C. Aime, I. V. Grigoriev, F. Martin, J.E. Stajich, M. Blackwell, The fungal tree of life: from molecular systematics to genome-scale phylogenies, Microbiol. Spectr. 5 (2017). https://doi.org/10.1128/microbiolspec.FUNK-0053-2016.

[3] J.E. Stajich, Fungal genomes and insights into the evolution of the kingdom, Microbiol. Spectr. 5 (2017). https://doi.org/10.1128/microbiolspec.FUNK-0055-2016.

[4] P. Baldrian, T. Větrovský, C. Lepinay, P. Kohout, High-throughput sequencing view on the magnitude of global fungal diversity, Fungal Divers. 114 (2022) 539–547. https://doi.org/10.1007/s13225-021-00472-y.

[5] D.L. Hawksworth, R. Lücking, Fungal diversity revisited: 2.2 to 3.8 million species, Microbiol. Spectr. 5 (2017). https://doi.org/10.1128/microbiolspec.FUNK-0052-2016.

[6] A. Amend, G. Burgaud, M. Cunliffe, V.P. Edgcomb, C.L. Ettinger, M.H. Gutiérrez, J. Heitman, E.F.Y. Hom, G. Ianiri, A.C. Jones, M. Kagami, K.T. Picard, C.A. Quandt, S. Raghukumar, M. Riquelme, J. Stajich, J. Vargas-Muñiz, A.K. Walker, O. Yarden, A.S. Gladfelter, Fungi in the marine environment: open questions and unsolved problems, MBio. 10 (2019) e01189-18. https://doi.org/10.1128/mBio.01189-

18.
[7] E.B.G. Jones, K.-L. Pang, M.A. Abdel-Wahab, B. Scholz, K.D. Hyde, T. Boekhout, R. Ebel, M.E. Rateb, L. Henderson, J. Sakayaroj, S. Suetrong, M.C. Dayarathne, V. Kumar, S. Raghukumar, K.R. Sridhar, A.H.A. Bahkali, F.H. Gleason, C. Norphanphoun, An online resource for marine fungi, Fungal Divers. 96 (2019) 347–433. https://doi.org/10.1007/s13225-019-00426-5.
[8] L.C. Reimer, J. Sardà Carbasse, J. Koblitz, C. Ebeling, A. Podstawka, J. Overmann, BacDive in 2022: the knowledge base for standardized bacterial and archaeal data, Nucleic Acids Res. 50 (2022) D741–D746. https://doi.org/10.1093/nar/gkab961.
[9] E.B.G. Jones, S. Suetrong, J. Sakayaroj, A.H. Bahkali, M.A. Abdel-Wahab, T. Boekhout, K.-L. Pang, Classification of marine Ascomycota, Basidiomycota, Blastocladiomycota and Chytridiomycota, Fungal Divers. 73 (2015) 1–72. https://doi.org/10.1007/s13225-015-0339-4.
[10] S. Banos, D.M. Gysi, T. Richter-Heitmann, F.O. Glöckner, M. Boersma, K.H. Wiltshire, G. Gerdts, A. Wichels, M. Reich, Seasonal dynamics of pelagic mycoplanktonic communities: Interplay of taxon abundance, temporal occurrence, and biotic interactions, Front. Microbiol. 11 (2020) 1305. https://doi.org/10.3389/fmicb.2020.01305.
[11] D.P. Overy, T. Rämä, R. Oosterhuis, A.K. Walker, K.-L. Pang, The neglected marine fungi, *sensu stricto*, and their isolation for natural products' discovery, Mar. Drugs. 17 (2019). https://doi.org/10.3390/md17010042.
[12] A. Kramer, A. Labes, 16 Biotechnology of Marine Fungi: New Workhorses and Applications BT - Genetics and Biotechnology, in: J.P. Benz, K. Schipper (Eds.), Springer International Publishing, Cham, 2020: pp. 399–412. https://doi.org/10.1007/978-3-030-49924-2_16.
[13] L. Balabanova, L. Slepchenko, O. Son, L. Tekutyeva, Biotechnology potential of marine fungi degrading plant and algae polymeric substrates, Front. Microbiol. 9 (2018) 1527. https://doi.org/10.3389/fmicb.2018.01527.
[14] A. Rokas, J.H. Wisecaver, A.L. Lind, The birth, evolution and death of metabolic gene clusters in fungi, Nat. Rev. Microbiol. (2018). https://doi.org/10.1038/s41579-018-0075-3.
[15] Y. Wang, D. Barth, A. Tamminen, M.G. Wiebe, Growth of marine fungi on polymeric substrates, BMC Biotechnol. 16 (2016) 3. https://doi.org/10.1186/s12896-016-0233-5.
[16] A. Kumar, J.L. Sørensen, F.T. Hansen, M. Arvas, M.F. Syed, L. Hassan, J.P. Benz, E. Record, B. Henrissat, S. Pöggeler, F. Kempken, Genome sequencing and analyses of two marinefungi from the North Sea unraveled a plethora of novel biosynthetic gene clusters, Sci. Rep. 8 (2018) 10187. https://doi.org/10.1038/s41598-018-28473-z.
[17] M. Bäumgen, T. Dutschei, U.T. Bornscheuer, Marine polysaccharides: occurrence, enzymatic degradation and utilization, ChemBioChem. 22 (2021) 2247–2256. https://doi.org/10.1002/cbic.202100078.
[18] A. Sichert, C.H. Corzett, M.S. Schechter, F. Unfried, S. Markert, D. Becher, A. Fernandez-Guerra, M. Liebeke, T. Schweder, M.F. Polz, J.-H. Hehemann, Verrucomicrobia use hundreds of enzymes to digest the algal polysaccharide fucoidan, Nat. Microbiol. 5 (2020) 1026–1039. https://doi.org/10.1038/s41564-020-0720-2.
[19] P.S. Kwon, H. Oh, S.-J. Kwon, W. Jin, F. Zhang, K. Fraser, J.J. Hong, R.J. Linhardt, J.S. Dordick, Sulfated polysaccharides effectively inhibit SARS-CoV-2 in vitro, Cell Discov. 6 (2020) 50. https://doi.org/10.1038/s41421-020-00192-8.

[20] S.-K. Yim, K. Kim, I. Kim, S. Chun, T. Oh, J.-U. Kim, J. Kim, W. Jung, H. Moon, B. Ku, K. Jung, Inhibition of SARS-CoV-2 virus entry by the crude polysaccharides of seaweeds and Abalone Viscera *In Vitro*, Mar. Drugs. 19 (2021) 219. https://doi.org/10.3390/md19040219.

[21] Y. Feng, T. Wassie, R. Gan, X. Wu, Structural characteristics and immunomodulatory effects of sulfated polysaccharides derived from marine algae, Crit. Rev. Food Sci. Nutr. (2022) 1–17. https://doi.org/10.1080/10408398.2022.2043823.

[22] W. Yao, H.-M. Qiu, K.-L. Cheong, S. Zhong, Advances in anti-cancer effects and underlying mechanisms of marine algae polysaccharides, Int. J. Biol. Macromol. 221 (2022) 472–485. https://doi.org/10.1016/j.ijbiomac.2022.09.055.

[23] M. Wang, S. Veeraperumal, S. Zhong, K.-L. Cheong, Fucoidan-derived functional oligosaccharides: Recent developments, preparation, and potential applications, Foods. 12 (2023). https://doi.org/10.3390/foods12040878.

[24] R. Kalra, X.A. Conlan, M. Goel, Fungi as a potential source of pigments: Harnessing filamentous fungi, Front. Chem. 8 (2020). https://doi.org/10.3389/fchem.2020.00369.

[25] P. Velez, J. Gasca-Pineda, M. Riquelme, Cultivable fungi from deep-sea oil reserves in the Gulf of Mexico: Genetic signatures in response to hydrocarbons, Mar. Environ. Res. 153 (2020) 104816. https://doi.org/10.1016/j.marenvres.2019.104816.

[26] S. Wiegand, M. Jogler, C. Boedeker, D. Pinto, J. Vollmers, E. Rivas-Marín, T. Kohn, S.H. Peeters, A. Heuer, P. Rast, S. Oberbeckmann, B. Bunk, O. Jeske, A. Meyerdierks, J.E. Storesund, N. Kallscheuer, S. Lücker, O.M. Lage, T. Pohl, B.J. Merkel, P. Hornburger, R.-W. Müller, F. Brümmer, M. Labrenz, A.M. Spormann, H.J.M. Op den Camp, J. Overmann, R. Amann, M.S.M. Jetten, T. Mascher, M.H. Medema, D.P. Devos, A.-K. Kaster, L. Øvreås, M. Rohde, M.Y. Galperin, C. Jogler, Cultivation and functional characterization of 79 planctomycetes uncovers their unique biology, Nat. Microbiol. 5 (2020) 126–140. https://doi.org/10.1038/s41564-019-0588-1.

[27] G. Burgaud, T. Le Calvez, D. Arzur, P. Vandenkoornhuyse, G. Barbier, Diversity of culturable marine filamentous fungi from deep-sea hydrothermal vents, Environ. Microbiol. 11 (2009) 1588–1600. https://doi.org/10.1111/j.1462-2920.2009.01886.x.

[28] L.C. Thomas, B. Gaëtan, M. Stéphane, B. Georges, V. Philippe, Fungal diversity in deep-sea hydrothermal ecosystems, Appl. Environ. Microbiol. 75 (2009) 6415–6421. https://doi.org/10.1128/AEM.00653-09.

[29] B.H. Conlon, S. Schmidt, M. Poulsen, J.Z. Shik, Orthogonal protocols for DNA extraction from filamentous fungi, STAR Protoc. 3 (2022) 101126. https://doi.org/10.1016/j.xpro.2022.101126.

[30] T.J. White, Amplification and direct sequencing of fungal ribosomal RNA genes for phylogenetics, in: M.A. Innis, D.H. Gelfand, J.J. Sninsky, T.J. White (Eds.), PCR Protoc. A Guid. to Methods Appl., Academic Press, 1990: pp. 315–322. https://doi.org/10.1016/B978-0-12-372180-8.50042-1.

[31] H. Toju, A.S. Tanabe, S. Yamamoto, H. Sato, High-coverage ITS primers for the DNA-based identification of Ascomycetes and Basidiomycetes in environmental samples, PLoS One. 7 (2012) e40863. https://doi.org/10.1371/journal.pone.0040863.

[32] E. Afgan, D. Baker, B. Batut, M. van den Beek, D. Bouvier, M. Čech, J. Chilton, D. Clements, N. Coraor, B.A. Grüning, A. Guerler, J. Hillman-Jackson, S. Hiltemann, V. Jalili, H. Rasche, N. Soranzo, J. Goecks, J. Taylor, A. Nekrutenko, D. Blankenberg, The Galaxy platform for accessible, reproducible and collaborative biomedical

analyses: 2018 update, Nucleic Acids Res. 46 (2018) W537–W544. https://doi.org/10.1093/nar/gky379.
[33] A. Bankevich, S. Nurk, D. Antipov, A.A. Gurevich, M. Dvorkin, A.S. Kulikov, V.M. Lesin, S.I. Nikolenko, S. Pham, A.D. Prjibelski, A. V Pyshkin, A. V Sirotkin, N. Vyahhi, G. Tesler, M.A. Alekseyev, P.A. Pevzner, SPAdes: A new genome assembly algorithm and its applications to single-cell sequencing, J. Comput. Biol. 19 (2012) 455–477. https://doi.org/10.1089/cmb.2012.0021.
[34] I. V Grigoriev, R. Nikitin, S. Haridas, A. Kuo, R. Ohm, R. Otillar, R. Riley, A. Salamov, X. Zhao, F. Korzeniewski, T. Smirnova, H. Nordberg, I. Dubchak, I. Shabalov, MycoCosm portal: gearing up for 1000 fungal genomes, Nucleic Acids Res. 42 (2014) D699–D704. https://doi.org/10.1093/nar/gkt1183.
[35] I. V Grigoriev, D. Cullen, S.B. Goodwin, D. Hibbett, T.W. Jeffries, C.P. Kubicek, C. Kuske, J.K. Magnuson, F. Martin, J.W. Spatafora, A. Tsang, S.E. Baker, Fueling the future with fungal genomics, Mycology. 2 (2011) 192–209. https://doi.org/10.1080/21501203.2011.584577.
[36] I. Letunic, P. Bork, Interactive Tree of Life (iTOL) v6: recent updates to the phylogenetic tree display and annotation tool, Nucleic Acids Res. 52 (2024) W78–W82. https://doi.org/10.1093/nar/gkae268.
[37] F.A. Simão, R.M. Waterhouse, P. Ioannidis, E. V Kriventseva, E.M. Zdobnov, BUSCO: assessing genome assembly and annotation completeness with single-copy orthologs, Bioinformatics. 31 (2015) 3210–3212. https://doi.org/10.1093/bioinformatics/btv351.
[38] M. Manni, M.R. Berkeley, M. Seppey, E.M. Zdobnov, BUSCO: Assessing genomic data quality and beyond, Curr. Protoc. 1 (2021) e323. https://doi.org/10.1002/cpz1.323.
[39] L.M. Rodriguez-R, K.T. Konstantinidis, The enveomics collection: a toolbox for specialized analyses of microbial genomes and metagenomes, PeerJ Prepr. 4 (2016) e1900v1. https://doi.org/10.7287/peerj.preprints.1900v1.
[40] A.J. Medlar, P. Törönen, L. Holm, AAI-profiler: fast proteome-wide exploratory analysis reveals taxonomic identity, misclassification and contamination, Nucleic Acids Res. 46 (2018) W479–W485. https://doi.org/10.1093/nar/gky359.
[41] H. Zhang, T. Yohe, L. Huang, S. Entwistle, P. Wu, Z. Yang, P.K. Busk, Y. Xu, Y. Yin, dbCAN2: a meta server for automated carbohydrate-active enzyme annotation, Nucleic Acids Res. 46 (2018) W95–W101. https://doi.org/10.1093/nar/gky418.
[42] J. Zheng, Q. Ge, Y. Yan, X. Zhang, L. Huang, Y. Yin, dbCAN3: automated carbohydrate-active enzyme and substrate annotation, Nucleic Acids Res. 51 (2023) W115–W121. https://doi.org/10.1093/nar/gkad328.
[43] E. Drula, M.-L. Garron, S. Dogan, V. Lombard, B. Henrissat, N. Terrapon, The carbohydrate-active enzyme database: functions and literature, Nucleic Acids Res. 50 (2022) D571–D577. https://doi.org/10.1093/nar/gkab1045.
[44] T. Barbeyron, L. Brillet-Guéguen, W. Carré, C. Carrière, C. Caron, M. Czjzek, M. Hoebeke, G. Michel, Matching the diversity of sulfated biomolecules: Creation of a classification database for sulfatases reflecting their substrate specificity, PLoS One. 11 (2016) e0164846. https://doi.org/10.1371/journal.pone.0164846.
[45] K. Blin, S. Shaw, H.E. Augustijn, Z.L. Reitz, F. Biermann, M. Alanjary, A. Fetter, B.R. Terlouw, W.W. Metcalf, E.J.N. Helfrich, G.P. van Wezel, M.H. Medema, T. Weber, antiSMASH 7.0: new and improved predictions for detection, regulation, chemical structures and visualisation, Nucleic Acids Res. (2023) gkad344. https://doi.org/10.1093/nar/gkad344.
[46] E. Käfer, Origins of translocations in *Aspergillus nidulans*, Genetics. 52 (1965)

217 LP – 232.
[47] T. Nayak, E. Szewczyk, C.E. Oakley, A. Osmani, L. Ukil, S.L. Murray, M.J. Hynes, S.A. Osmani, B.R. Oakley, A versatile and efficient gene-targeting system for *Aspergillus nidulans*, Genetics. 172 (2006) 1557–66.
[48] T. Metsalu, J. Vilo, ClustVis: a web tool for visualizing clustering of multivariate data using Principal Component Analysis and heatmap, Nucleic Acids Res. 43 (2015) W566–W570. https://doi.org/10.1093/nar/gkv468.
[49] D.G. Drubin, K.G. Miller, D. Botstein, Yeast actin-binding proteins: evidence for a role in morphogenesis., J. Cell Biol. 107 (1988) 2551–2561. https://doi.org/10.1083/jcb.107.6.2551.
[50] J.R. Wiśniewski, A. Zougman, N. Nagaraj, M. Mann, Universal sample preparation method for proteome analysis, Nat. Methods. 6 (2009) 359–362. https://doi.org/10.1038/nmeth.1322.
[51] V. Demichev, C.B. Messner, S.I. Vernardis, K.S. Lilley, M. Ralser, DIA-NN: neural networks and interference correction enable deep proteome coverage in high throughput, Nat.Methods.17 (2020) 41–44. https://doi.org/10.1038/s41592-019-0638-x.
[52] S. Tyanova, T. Temu, P. Sinitcyn, A. Carlson, M.Y. Hein, T. Geiger, M. Mann, J. Cox, The Perseus computational platform for comprehensive analysis of (prote)omics data, Nat. Methods. 13 (2016) 731–740. https://doi.org/10.1038/nmeth.3901.
[53] S. Mongkolsamrit, A. Khonsanit, D. Thanakitpipattana, K. Tasanathai, W. Noisripoom, S. Lamlertthon, W. Himaman, J. Houbraken, R.A. Samson, J. Luangsa-ard, Revisiting *Metarhizium* and the description of new species from Thailand, Stud. Mycol. 95 (2020) 171–251. https://doi.org/10.1016/j.simyco.2020.04.001.
[54] R.A. Samson, *Paecilomyces* and some allied Hyphomycetes, Stud. Mycol. 6 (1974) 1–119.
[55] I. Skromne, O. Sanchez, J. Aguirre, Starvation stress modulates the expression of the *Aspergillus nidulans brlA* regulatory gene, Microbiology. 141 (1995) 21–28. https://doi.org/10.1099/00221287-141-1-21.
[56] O. Etxebeste, A. Markina-Iãrrairaegui, A. Garzia, E. Herrero-García, U. Ugalde, E.A. Espeso, Kapl, a non-essential member of the Pse1p/Imp5 karyopherin family, controls colonial and asexual development in *Aspergillus nidulans*, Microbiology. 155 (2009) 3934–3945.
[57] M.T. Ale, J.D. Mikkelsen, A.S. Meyer, Important determinants for fucoidan bioactivity: A critical review of structure-function relations and extraction methods for Fucose-Containing Sulfated Polysaccharides from brown seaweeds, Mar. Drugs. 9 (2011). https://doi.org/10.3390/md9102106.
[58] Y. Zhao, Y. Zheng, J. Wang, S. Ma, Y. Yu, W.L. White, S. Yang, F. Yang, J. Lu, Fucoidan extracted from *Undaria pinnatifida*: Source for nutraceuticals/functional foods, Mar. Drugs. 16 (2018). https://doi.org/10.3390/md16090321.
[59] H.S.A. Koh, J. Lu, W. Zhou, Structure characterization and antioxidant activity of fucoidan isolated from *Undaria pinnatifida* grown in New Zealand, Carbohydr. Polym. 212 (2019) 178–185. https://doi.org/10.1016/j.carbpol.2019.02.040.
[60] W.-Y. Jia, J.-J. Xu, T.-P. Wei, M.-Y. Luo, H. Zhang, Y.-L. Jiang, *Albophoma* belongs in Ophiocordycipitaceae, with a new record from China, Mycotaxon. 137 (2022) 537–543. https://doi.org/10.5248/137.537.
[61] R. Uchida, R. Imasato, Y. Yamaguchi, R. Masuma, K. Shiomi, H. Tomoda, S. Ōmura, New Sesquicillins, insecticidal antibiotics produced by *Albophoma sp*. FKI-1778, J. Antibiot. (Tokyo). 58 (2005) 397–404. https://doi.org/10.1038/ja.2005.50.

[62] T. Kobayashi, R. Masuma, S. Omura, K. Watanabe, Materials for the fungus flora of Japan (47), Mycoscience. 35 (1994) 399–401. https://doi.org/10.1007/BF02268512.

[63] X. Huang, H. Tomoda, H. Nishida, R. Masuma, S. Omura, Terpendoles, novel ACAT inhibitors produced by *Albophoma yamanashiensis*. I. Production, isolation and biological properties, J. Antibiot. (Tokyo). 48 (1995) 1–4. https://doi.org/10.7164/antibiotics.48.1.

[64] P.G. Arnison, M.J. Bibb, G. Bierbaum, A.A. Bowers, T.S. Bugni, G. Bulaj, J.A. Camarero, D.J. Campopiano, G.L. Challis, J. Clardy, P.D. Cotter, D.J. Craik, M. Dawson, E. Dittmann, S. Donadio, P.C. Dorrestein, K.-D. Entian, M.A. Fischbach, J.S. Garavelli, U. Göransson, C.W. Gruber, D.H. Haft, T.K. Hemscheidt, C. Hertweck, C. Hill, A.R. Horswill, M. Jaspars, W.L. Kelly, J.P. Klinman, O.P. Kuipers, A.J. Link, W. Liu, M.A. Marahiel, D.A. Mitchell, G.N. Moll, B.S. Moore, R. Müller, S.K. Nair, I.F. Nes, G.E. Norris, B.M. Olivera, H. Onaka, M.L. Patchett, J. Piel, M.J.T. Reaney, S. Rebuffat, R.P. Ross, H.-G. Sahl, E.W. Schmidt, M.E. Selsted, K. Severinov, B. Shen, K. Sivonen, L. Smith, T. Stein, R.D. Süssmuth, J.R. Tagg, G.-L. Tang, A.W. Truman, J.C. Vederas, C.T. Walsh, J.D. Walton, S.C. Wenzel, J.M. Willey, W.A. van der Donk, Ribosomally synthesized and post-translationally modified peptide natural products: overview and recommendations for a universal nomenclature, Nat. Prod. Rep. 30 (2013) 108–160. https://doi.org/10.1039/C2NP20085F.

[65] H. Li, W. Ding, Q. Zhang, Discovery and engineering of ribosomally synthesized and post-translationally modified peptide (RiPP) natural products, RSC Chem. Biol. 5 (2024) 90–108. https://doi.org/10.1039/D3CB00172E.

[66] C.D. Reeves, Z. Hu, R. Reid, J.T. Kealey, Genes for the biosynthesis of the fungal polyketides hypothemycin from *Hypomyces subiculosus* and radicicol from *Pochonia chlamydosporia*, Appl. Environ. Microbiol. 74 (2008) 5121–5129. https://doi.org/10.1128/AEM.00478-08.

[67] M. Nishino, J.W. Choy, N.N. Gushwa, J.A. Oses-Prieto, K. Koupparis, A.L. Burlingame, A.R. Renslo, J.H. McKerrow, J. Taunton, Hypothemycin, a fungal natural product, identifies therapeutic targets in *Trypanosoma brucei*, Elife. 2 (2013) e00712. https://doi.org/10.7554/eLife.00712.

[68] G. Chen, J. Chu, Characterization of two polyketide synthases involved in sorbicillinoid biosynthesis by *Acremonium chrysogenum* using the CRISPR/Cas9 system, Appl. Biochem. Biotechnol. 188 (2019) 1134–1144. https://doi.org/10.1007/s12010-019-02960-z.

[69] W.-Y. Zhang, Y. Zhong, Y. Yu, D.-F. Shi, H.-Y. Huang, X.-L. Tang, Y.-H. Wang, G.-D. Chen, H.-P. Zhang, C.-L. Liu, D. Hu, H. Gao, X.-S. Yao, 4-Hydroxy pyridones from heterologous expression and cultivation of the native host, J. Nat. Prod. 83 (2020) 3338–3346. https://doi.org/10.1021/acs.jnatprod.0c00675.

[70] B. Li, F. Lu, X. Wei, R. Zhao, Fucoidan: Structure and bioactivity, Molecules. 13 (2008) 1671–1695. https://doi.org/10.3390/molecules13081671.

[71] S. Khalid, J.A. Baccile, J.E. Spraker, J. Tannous, M. Imran, F.C. Schroeder, N.P. Keller, NRPS-derived isoquinolines and lipopetides mediate antagonism between plant pathogenic fungi and bacteria, ACS Chem. Biol. 13 (2018) 171–179. https://doi.org/10.1021/acschembio.7b00731.

[72] G.M. Cabrera, M. Butler, M.A. Rodriguez, A. Godeas, R. Haddad, M.N. Eberlin, A Sorbicillinoid Urea from an intertidal *Paecilomyces marquandii*, J. Nat. Prod. 69 (2006) 1806–1808. https://doi.org/10.1021/np060315d.

[73] J.T. Staley, A. Konopka, Measurement of *in situ* activities of nonphotosynthetic microorganisms in aquatic and terrestrial habitats, Annu. Rev. Microbiol. 39 (1985)

321–346. https://doi.org/10.1146/annurev.mi.39.100185.001541.
[74] M.K. da Silva, L.M.D. de Souza, R. Vieira, A.A. Neto, F.A.C. Lopes, F.S. de Oliveira, P. Convey, M. Carvalho-Silva, A.W.F. Duarte, P.E.A.S. Câmara, L.H. Rosa, Fungal and fungal-like diversity in marine sediments from the maritime Antarctic assessed using DNA metabarcoding, Sci. Rep. 12 (2022) 21044. https://doi.org/10.1038/s41598-022-25310-2.
[75] M.B. Ogaki, O.H.B. Pinto, R. Vieira, A.A. Neto, P. Convey, M. Carvalho-Silva, C.A. Rosa, P.E.A.S. Câmara, L.H. Rosa, Fungi present in Antarctic deep-sea sediments assessed using DNA Metabarcoding, Microb. Ecol. 82 (2021) 157–164. https://doi.org/10.1007/s00248-020-01658-8.
[76] M.T. Robey, L.K. Caesar, M.T. Drott, N.P. Keller, N.L. Kelleher, An interpreted atlas of biosynthetic gene clusters from 1,000 fungal genomes, Proc. Natl. Acad. Sci. 118 (2021) e2020230118. https://doi.org/10.1073/pnas.2020230118.
[77] N. Khaldi, F.T. Seifuddin, G. Turner, D. Haft, W.C. Nierman, K.H. Wolfe, N.D. Fedorova, SMURF: Genomic mapping of fungal secondary metabolite clusters, Fungal Genet. Biol. 47 (2010) 736–741. https://doi.org/10.1016/j.fgb.2010.06.003.
[78] J. Nakazawa, J. Yajima, T. Usui, M. Ueki, A. Takatsuki, M. Imoto, Y.Y. Toyoshima, H. Osada, A novel action of Terpendole E on the motor activity of mitotic kinesin Eg5, Chem. Biol. 10 (2003) 131–137. https://doi.org/10.1016/S1074-5521(03)00020-6.
[79] A.M. Harned, K.A. Volp, The sorbicillinoid family of natural products: Isolation, biosynthesis, and synthetic studies, Nat. Prod. Rep. 28 (2011) 1790–1810. https://doi.org/10.1039/C1NP00039J.
[80] P. Zhang, Y. Deng, X. Lin, B. Chen, J. Li, H. Liu, S. Chen, L. Liu, Anti-inflammatory mono- and dimeric Sorbicillinoids from the marine-derived fungus *Trichoderma reesei* 4670, J. Nat. Prod. 82 (2019) 947–957. https://doi.org/10.1021/acs.jnatprod.8b01029.
[81] J. Meng, X. Wang, D. Xu, X. Fu, X. Zhang, D. Lai, L. Zhou, G. Zhang, Sorbicillinoids from fungi and their bioactivities, Molecules. 21 (2016) 715. https://doi.org/10.3390/molecules21060715.
[82] C. Li, R. Gu, F. Lin, H. Xiao, Sorbicillinoids hyperproduction without affecting the cellulosic enzyme production in *Trichoderma reesei* JNTR5, Biotechnol. Biofuels Bioprod. 15 (2022) 85. https://doi.org/10.1186/s13068-022-02183-1.
[83] F. Guzmán-Chávez, O. Salo, Y. Nygård, P.P. Lankhorst, R.A.L. Bovenberg, A.J.M. Driessen, Mechanism and regulation of sorbicillin biosynthesis by *Penicillium chrysogenum*, Microb. Biotechnol. 10 (2017) 958–968. https://doi.org/10.1111/1751-7915.12736.
[84] C. Derntl, F. Guzmán-Chávez, T.M. Mello-de-Sousa, H.-J. Busse, A.J.M. Driessen, R.L. Mach, A.R. Mach-Aigner, *In vivo* study of the sorbicillinoid gene cluster in *Trichoderma reesei*, Front. Microbiol. 8 (2017). https://doi.org/10.3389/fmicb.2017.02037.
[85] A. Cartmell, J. Muñoz-Muñoz, J.A. Briggs, D.A. Ndeh, E.C. Lowe, A. Baslé, N. Terrapon, K. Stott, T. Heunis, J. Gray, L. Yu, P. Dupree, P.Z. Fernandes, S. Shah, S.J. Williams, A. Labourel, M. Trost, B. Henrissat, H.J. Gilbert, Author Correction: A surface endogalactanase in *Bacteroides thetaiotaomicron* confers keystone status for arabinogalactan degradation, Nat. Microbiol. 4 (2019) 2021–2023. https://doi.org/10.1038/s41564-019-0584-5.
[86] C. Pérez-Cruz, A. Moraleda-Montoya, R. Liébana, O. Terrones, U. Arrizabalaga, M. García-Alija, M. Lorizate, A. Martínez Gascueña, I. García-Álvarez, J.A. Nieto-Garai, J. Olazar-Intxausti, B. Rodríguez-Colinas, E. Mann, J.L. Chiara, F.-X.

Contreras, M.E. Guerin, B. Trastoy, L. Alonso-Sáez, Mechanisms of recalcitrant fucoidan breakdown in marine Planctomycetota, Nat. Commun. 15 (2024) 10906. https://doi.org/10.1038/s41467-024-55268-w.

[87] B.X. Wang, C.M. Wu, K. Ribbeck, Home, sweet home: how mucus accommodates our microbiota, FEBS J. 288 (2021) 1789–1799. https://doi.org/10.1111/febs.15504.

[88] A. Cartmell, E.C. Lowe, A. Baslé, S.J. Firbank, D.A. Ndeh, H. Murray, N. Terrapon, V. Lombard, B. Henrissat, J.E. Turnbull, M. Czjzek, H.J. Gilbert, D.N. Bolam, How members of the human gut microbiota overcome the sulfation problem posed by glycosaminoglycans, Proc. Natl. Acad. Sci. 114 (2017) 7037–7042. https://doi.org/10.1073/pnas.1704367114.

[89] C.S. Robb, J.K. Hobbs, B. Pluvinage, G. Reintjes, L. Klassen, S. Monteith, G. Giljan, C. Amundsen, C. Vickers, A.G. Hettle, R. Hills, Nitin, X. Xing, T. Montina, W.F. Zandberg, D.W. Abbott, A.B. Boraston, Metabolism of a hybrid algal galactan by members of the human gut microbiome, Nat. Chem. Biol. 18 (2022) 501–510. https://doi.org/10.1038/s41589-022-00983-y.

[90] R. Garcia-Rubio, H.C. de Oliveira, J. Rivera, N. Trevijano-Contador, The fungal cell wall: *Candida*, *Cryptococcus*, and *Aspergillus* species, Front. Microbiol. 10 (2020) 1–13. https://doi.org/10.3389/fmicb.2019.02993.

[91] N.A.R. Gow, M.D. Lenardon, Architecture of the dynamic fungal cell wall, Nat. Rev. Microbiol. 21 (2023) 248–259. https://doi.org/10.1038/s41579-022-00796-9.

Table 1: General data for genome sequencing analyses of isolates M60 and M98. C: Complete BUSCOs; S: Complete and single-copy BUSCOs; D: Complete and duplicated BUSCOs; F: Fragmented BUSCOs; M: Missing BUSCOs; n: Total number of BUSCOs for Hypocreales.

Isolate	**Assembly (Spades)**						**Annotation**	**BUSCO (%)**					
	Size (Mb)	***Contigs* (> 2000 bp)**	***Contigs* (all)**	**N50 (Mbp)**	**L50**	**Largest *contig* (Mbp)**	**Number of gene models**	**C**	**S**	**D**	**F**	**M**	**n**
M60	43.61	97	461	2,52	6	5,62	12,408	97.2	96.2	1.0	0.4	2.4	4494
M98	31.18	38	139	3,37	4	4,47	10,216	97.2	96.4	0.8	0.4	2.4	4494

Figures.

Figure 1: Geographic location of the seven sampling points along the Basque coast selected in this work. Circles indicate estuaries while the square indicates a coastal area. EOK: river Oka; EA: river Artibai; EU: river Urola; EO: river Oria; LUR: river Urumea; EOI: river Oiartzun.

Figure 2: Phenotypic characterization of the library of filamentous microbes isolated from sediments collected along the Basque coast. The Sankey diagram shows A) the number of isolates obtained from each sediment sample (see Figure 1 and section 2), and B) the classes and genera represented in the subset of isolates whose ITS and/or *rpb1* regions were amplified (PCR) and Sanger-sequenced. C) Phenotypes of a random subset of isolates of our collection on the same culture medium (PDA, MEA, CMA, Pc or Lc) used for their isolation (see also Figure S2). The diameter of plates is 5.5 cm.

Figure 3: Phenotypic characterization of isolate M60 (*M. marquandii*). A) Lateral view of the culture plates (left) and phenotypes of some of the isolates (right) staining the culture medium due to the secretion of pigments, in MEA culture medium**.** The light blue square corresponds to isolate M60. B) Up: Developmental structures produced by *M. marquandii*. Scale bars: 1 mm. Down: Microscopy images showing germlings, mature hyphae and conidia. Scale bars: 5 µm. C) Phenotype and colony diameters of *M. marquandii* on MEA, PDA and MMM media after 0, 3, 7, 12 and 16 days of culture at 25º C. Values are calculated as the average ± standard deviation of three replicates per culture medium. Scale bar: 1 cm. D) Phenotype and colony diameters of *M. marquandii* on MEA, PDA and MMM media after 0, 5, 10 and 15 days of culture at 25º, 30º, 35º and 37º C. Diameter of Petri plates is 5.5 cm. Values on the graphs are calculated as the average ± standard deviation of three replicates per culture medium and temperature. E)

OD_{380nm} values for the supernatants of *M. marquandii* cultures, measured daily (16 days) as the average ± sd of three replicates. Cultures were grown at 25º C. F) Phenotypes (up) and contact zones (down) between *M. marquandii* and *A. nidulans* on MEA, PDA and MMA media at 25º C. Scale bar: 1 cm. G) Phenotypes (top views in both rows 1 and 2) and contact zones (row 3) between *M. marquandii* and isolate M98 (*A. yamanashiensis*; left), isolate M122 (*genus Acrostalagmus*; middle) and isolate MFuc12 (*genus Gliomastix*; right) on MEA and PDA media at 25º C. See Experimental section for the time of inoculation of each species. Scale bar: 1 cm.

Figure 4: Phenotypic characterization of isolate M98. A) Phenotype on minimal medium supplemented with glucose or fucoidan from *Fucus vesiculosus* or *Undaria pinnatifida* (see Experimental section; see also Figure S5). B) Phenotype of M98 in MEA medium (scale bar: 1 cm), with the formation of pycnidia in panel C (scale bars, 1 and 0.1 mm, respectively). D) Phenotype and colony diameters on MEA, PDA and MMM media after 0, 5, 10 and 15 days of culture at 25º, 30º, 35º and 37º C. Diameter of Petri plates is 5.5 cm. Values on the graphs are calculated as the average ± standard deviation of three replicates per culture medium and temperature.

Figure 5: Genomics analyses of isolates M60 and M98. A) ANI analysis in which the genomes of M60 and M98 were compared to those of multiple Hypocreales species (see Table S1). B) Counts for genes encoding backbone enzymes of secondary metabolite gene clusters in the genomes of specific species of the order Hypocreales. The data in the heatmaps was retrieved from antiSMASH. C) Predicted CAZyme repertoires of isolates M60 and M98. The heatmap was generated using the data given by the MycoCosm annotation pipeline. Brown squares highlight GH families used by marine bacteria for fucoidan degradation [18]. For panels B and C, the trees in the heatmaps were generated with the common tree function at the NCBI taxonomy browser, using

the IDs of the species analyzed. Red squares highlight data corresponding to *M. marquandii* and *A. yamanashiensis*.

Figure 6: Transcriptional profiling of isolate M60 in PDB and MEB culture media. A) Correlation among the replicates (two per culture medium) analyzed. B) PCA plot for the replicates. C) MA plot showing genes up- and downregulated in PDB compared to MEB media. D) Heatmap showing the expression values for the Top100 up- and downregulated genes. E) GO enrichment analysis for genes up- (left) and downregulated (right) in PDB compared to MEB media. F) Functional analysis of Top20 up- and downregulated genes in PDB compared to MEB media. G) Ratios corresponding to the number of significantly deregulated genes in each secondary metabolite gene cluster and the number of cluster genes, in PDB versus MEB media. The list of genes from each secondary metabolite gene cluster were predicted by antiSMASH. Purple squares indicate clusters composed of more than ten genes and in which more than 35% of those genes were significantly deregulated in PDB compared to MEB. H) Gene organization in each of the secondary metabolite gene clusters highlighted in panel G. The color code corresponds to log2FC values. The predicted roles of the proteins encoded by cluster c6.5, predictably involved in the synthesis of a sorbicillinoid compound, are also included.

Figure 7: Transcriptional profilling of isolate M98 in culture medium supplemented with mannose or fucoidan. A) PCA plot for the nine samples sequenced. Mann: the three replicates for mycelia cultured with mannose as the main carbon source. FV: replicates for mycelia cultured with fucoidan from *F. vesiculosus*. UP: replicates for mycelia cultured with fucoidan from *U. pinnatifida*. B) Pearson correlation for the samples. C) MA plots showing genes up- and downregulated in three comparisons: FV Vs Mann, UP Vs Mann and UP Vs FV. D) Heatmap showing the expression patterns of

genes differentially expressed in FV_Vs_Mann and UP_Vs_Mann comparisons. Multiple expression patterns are highlighted by the dotted squares. E) Venn diagram for up- (left) and downregulated genes in FV_Vs_Mann and UP_Vs_Mann comparisons, showing the number of genes differentially expressed in both comparisons or in one of them.

Figure 8: Top20 genes in each of the three transcriptomics comparisons carried out in this work with *A. yamanashiensis*. Count and fold change (log2FC) values are shown, together with the characteristic domains identified by InterPro.

Figure 9: Comparison of transcriptomics and proteomics analyses of *A. yamanashiensis*. A) PCA plot for the nine crude protein samples sequenced. Mann: the three replicates for mycelia cultured with mannose as the main carbon source. FV: replicates for mycelia cultured with fucoidan from *F. vesiculosus*. UP: replicates for mycelia cultured with fucoidan from *U. pinnatifida*. B) Pearson correlation for the protein samples. C) Heatmap for proteins with statistically significant changes ($p < 0.05$; Top300 of each comparison, FV_Vs_Mann and UP_Vs_Mann) in their levels when isolate M98 is cultured on media supplemented with mannose or fucoidan from *F. vesiculosus* or *U. pinnatifida* as the carbon source. The dotted squares highlight groups of proteins with higher/lower levels only with fucoidan from *F. vesiculosus*, only with fucoidan from *U. pinnatifida*, or with both types of fucoidan. D) Venn diagrams showing the number of *A. yamanashiensis* proteins upregulated and downregulated in FV_Vs_Mann, UP_Vs_Mann or in both comparisons, when considering Top20 proteins or proteins with FV/Mann or UP/Mann ratios higher than 10 (UpReg) and below 0.1 (DwReg). E) CAZyme (dbCAN3) and sulfatase (SulfAtlas) analyses for the proteins and genes significantly upregulated in our proteomics and/or transcriptomics analyses. All genes and proteins (see Venn diagrams) with p values below 0.05 in the

FV_Vs_Mann (top) and UP_Vs_Mann (bottom) comparisons were considered. Those proteins with ratios >10 and/or those genes with log2FC values >3 are marked with asterisks (an 1,2-α-L-fucosidase of the GH95 family is also highlighted). The same color code as in Figure 5D was used to designate CAZyme categories (plus S for sulfatases; in red). FV/Mann and UV/Mann ratios correspond to $2^{\text{exp (value FV – value Mann)}}$, $2^{\text{exp (value UP – value Mann)}}$ and $2^{\text{exp (value UP – value FV)}}$, respectively.

Figure 10: Top20 proteins in each of the three proteomics comparisons carried out in this work with *A. yamanshiensis*. FV/Mann, UV/Mann and UP/FV ratios correspond to $2^{\text{exp (value FV – value Mann)}}$, $2^{\text{exp (value UP – value Mann)}}$ and $2^{\text{exp (value UP – value FV)}}$, respectively.

Supplementary Figures.

Figure S1: Phenotype of a subset of isolates of our library in minimal medium with decreasing concentrations of bacteriological agar, without (left column) and with (right column) glucose (2%). Considering the phenotype of the strains and solidification of the agar, a 0.5% concentration was selected for the subsequent phenotypic characterization of the isolates.

Figure S2: Phenotypes of a subset of 235 isolates of our library in PDA, MEA, Pc and Lc culture media, all supplemented with penicillin, grown at 25º C in the dark. Squares highlight isolates probably corresponding to the same strain (*e.g.*, isolates M106, M107 and M108) or different strains of the same species (*e.g.*, isolates M43, M44, M45 and M60).

Figure S3: Phenotype of selected isolates on plates filled with minimal medium supplemented with glucose, laminarin, alginate or fucoidan from *Laminaria japonica*, or without supplementation of any of these carbohydrate sources (negative control).

Figure S4: Phenotype of selected isolates on plates filled with minimal medium supplemented with 2 g/L of glucose or fucoidan from *Fucus vesiculosus* or *Undaria pinnatifida*, or without supplementation of any of these carbohydrate sources (negative control).

Figure S5: A) Phenotype of isolates M98 and M127 on minimal medium supplemented with laminarin or fucoidan from *Fucus vesiculosus* or *Undaria pinnatifida*, compared to the phenotype on MEA medium, MMM or MMM supplemented with glucose. Ammonium tartrate and sodium nitrate were tested as the main nitrogen source. glc: glucose; lam: laminarin; fucoi: fucoidan. Six-well plates were used.

Figure S6: A) KOG analyses of the genomes of M60 and M98 in comparison with specific Hypocreales species. All the data in the heatmap was retrieved from MycoCosm. C) Counts for genes encoding backbone enzymes of secondary metabolite gene clusters in the genomes of specific species of the order Hypocreales (plus the Eurotiales *P. niveus* and *P. variotii*). The data in the heatmap was retrieved from MycoCosm. For both panels, the trees in the heatmaps were generated with the common tree function at the NCBI taxonomy browser, using the IDs of the species analyzed. Red squares highlight data corresponding to *M. marquandii* and *A. yamanashiensis*.

Figure S7: Table showing the results obtained in the analysis of the potential secondary metabolite gene clusters predicted in the genome of isolate M60 (*Marquandomyces marquandii*) by antiSMASH. The table includes the node the potential cluster is located in, the backbone enzyme(s) of each cluster, coordinates, the most similar known cluster, the type of metabolite predictably synthesized and the similarity with the reference cluster. Similarity, in this case, refers to the percentage of genes within the closest known cluster that have a significant BLAST hit to genes within the predicted cluster

Figure S8: Table showing the results obtained in the analysis of the potential secondary metabolite gene clusters predicted in the genome of isolate M98 (*Albophoma yamanashiensis*) by antiSMASH.

Figure S9: CAZyme and sulfatase analyses for the proteins and genes significantly downregulated in our proteomics and/or transcriptomics analyses. All genes and proteins with p values below 0.05 in the FV_Vs_Mann (top) and UP_Vs_Mann (bottom) comparisons were considered (see Venn diagrams). Those proteins with ratios <0.1 and/or those genes with log2FC values <-3 are marked with asterisks. The same color code as in Figure 5D was used to designate CAZyme categories (plus S for sulfatases).

Supplementary Tables.

Table S1: Genomes used as reference in ANI analyses. GenBank and BioSample accession numbers are included.

Table S2: Predicted CAZYme repertoire for isolate M60. The analysis was carried out at the dbCAN website (Zhang *et al.*, 2018), and the table includes the CAZYme family each protein is linked to, the enzyme commission (EC) number, the tools that predicted this association as well as the hypothetic presence of a signal peptide in each predicted CAZYme.

Table S3: Predicted CAZYme repertoire for isolate M98.

Table S4: Differentially expressed genes of *M. marquandii* in PDB versus MEB media.

Table S5: Differentially expressed genes of *A. yamanashiensis* in medium supplemented with fucoidan from *F. vesiculosus* versus mannose as the main carbon source.

Table S6: Differentially expressed genes of *A. yamanashiensis* in medium supplemented with fucoidan from *U. pinnatifida* versus mannose as the main carbon source.

Table S7: Differentially expressed genes of *A. yamanashiensis* in medium supplemented with fucoidan from *U. pinnatifida* versus fucoidan from *F. vesiculosus*.

Table S8: Proteins of *A. yamanashiensis* with statistically significant changes in their levels when the minimal culture medium was supplemented with: 1) fucoidan from *F. vesiculosus* as the main carbon source compared to a medium supplemented with mannose; 2) fucoidan from *U. pinnatifida* as the main carbon source was compared to a medium supplemented with mannose; and 3) fucoidan from *U. pinnatifida* as the main carbon source was compared to a medium supplemented with fucoidan from *F. vesiculosus*. FV/Mann ratios correspond to $2^{\text{exp (value FV – value Mann)}}$, UP/Mann ratios correspond to $2^{\text{exp (value UP – value Mann)}}$, and UP/FV ratios correspond to $2^{\text{exp (value UP – value FV)}}$.

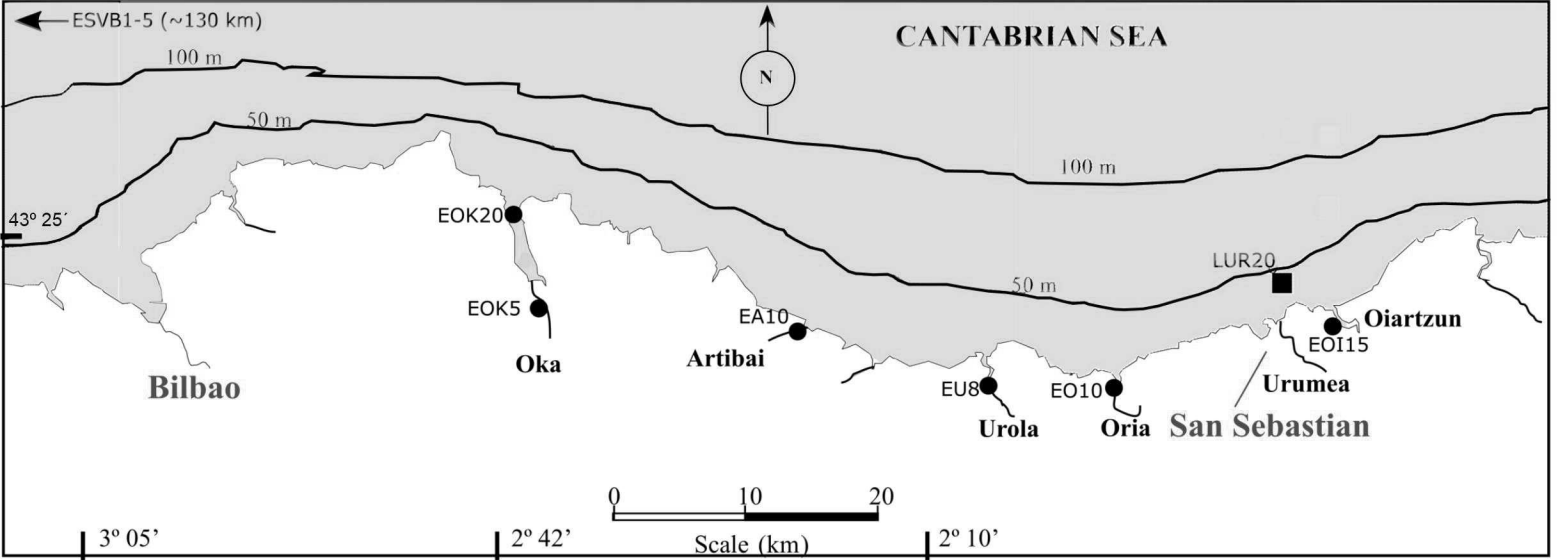
ESVB1-5 (~130 km)
CANTABRIAN SEA
N
100 m
50 m
100 m
50 m
43º 25´
EOK20
EOK5
Oka
EA10
Artibai
Bilbao
EU8
Urola
EO10
Oria
LUR20
Oiartzun
EOI15
Urumea
San Sebastian
0
10
20
Scale (km)
3º 05'
2º 42'
2º 10'

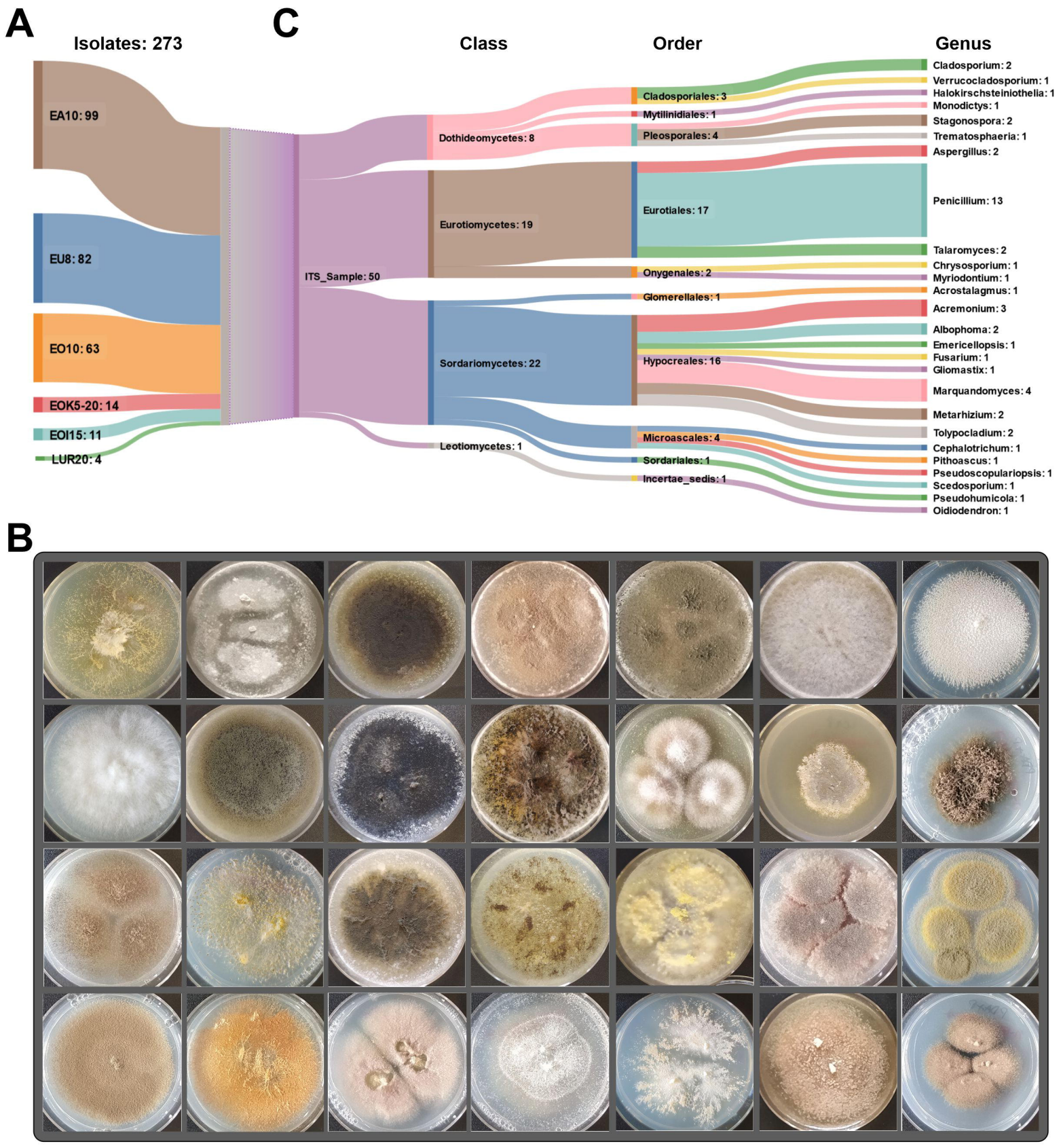
A
C
B
Isolates: 273
Class
Order
Genus
EA10: 99
EU8: 82
EO10: 63
EOK5-20: 14
EOI15: 11
LUR20: 4
ITS_Sample: 50
Dothideomycetes: 8
Eurotiomycetes: 19
Sordariomycetes: 22
Leotiomycetes: 1
Cladosporiales: 3
Mytilinidiales: 1
Pleosporales: 4
Eurotiales: 17
Onygenales: 2
Glomerellales: 1
Hypocreales: 16
Microascales: 4
Sordariales: 1
Incertae_sedis: 1
Cladosporium: 2
Verrucocladosporium: 1
Halokirschsteiniothelia: 1
Monodictys: 1
Stagonospora: 2
Trematosphaeria: 1
Aspergillus: 2
Penicillium: 13
Talaromyces: 2
Chrysosporium: 1
Myriodontium: 1
Acrostalagmus: 1
Acremonium: 3
Albophoma: 2
Emericellopsis: 1
Fusarium: 1
Gliomastix: 1
Marquandomyces: 4
Metarhizium: 2
Tolypocladium: 2
Cephalotrichum: 1
Pithoascus: 1
Pseudoscopulariopsis: 1
Scedosporium: 1
Pseudohumicola: 1
Oidiodendron: 1

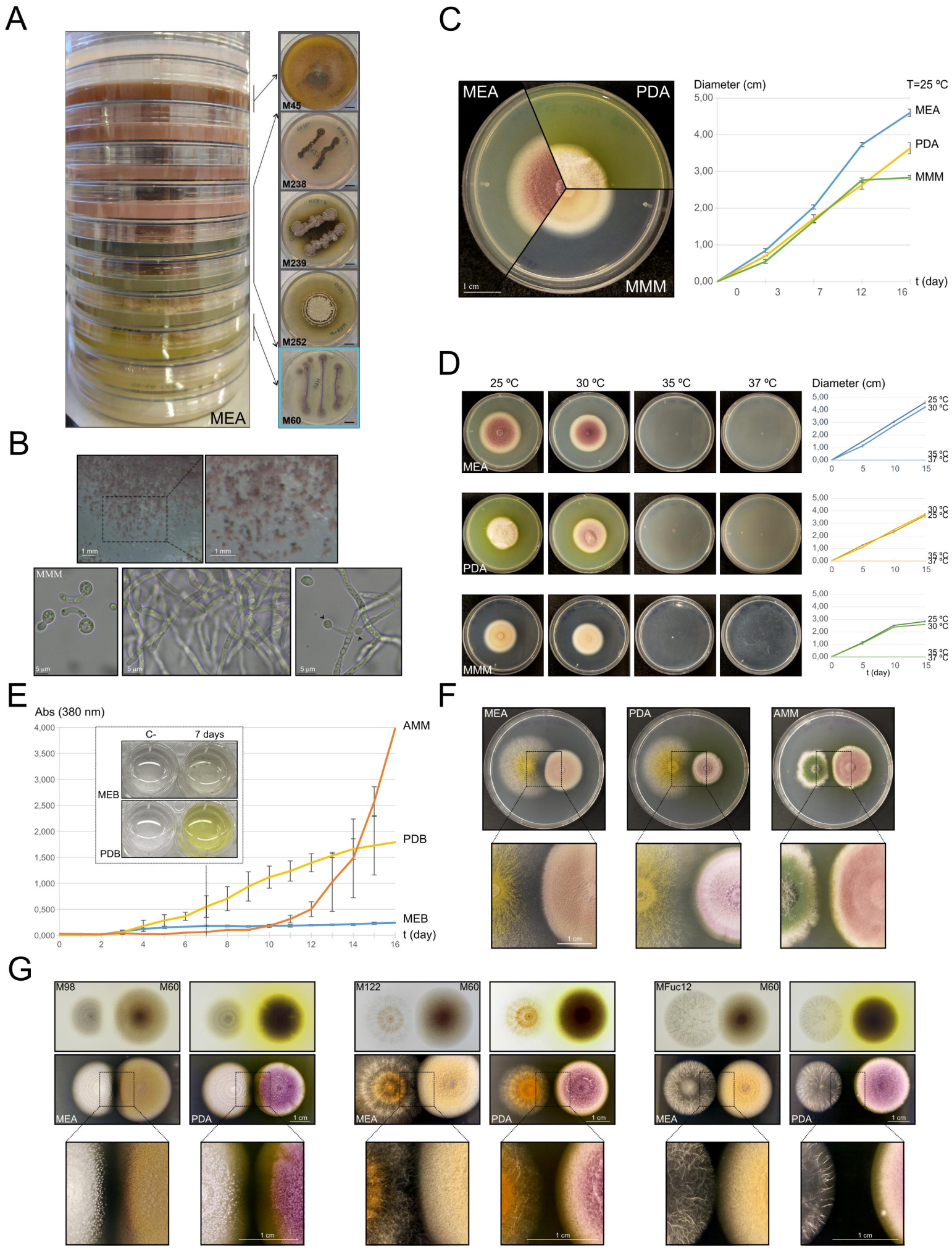
A
MEA
M45
M238
M239
M252
M60
B
1 mm
1 mm
MMM
5 µm
5 µm
5 µm
C
MEA
PDA
MMM
1 cm
Diameter (cm)
T=25 ºC
MEA
PDA
MMM
t (day)
D
25 ºC
30 ºC
35 ºC
37 ºC
Diameter (cm)
MEA
PDA
MMM
t (day)
E
Abs (380 nm)
C-
7 days
MEB
PDB
AMM
PDB
MEB
t (day)
F
MEA
PDA
AMM
1 cm
G
M98
M60
M122
M60
MFuc12
M60
MEA
PDA
1 cm

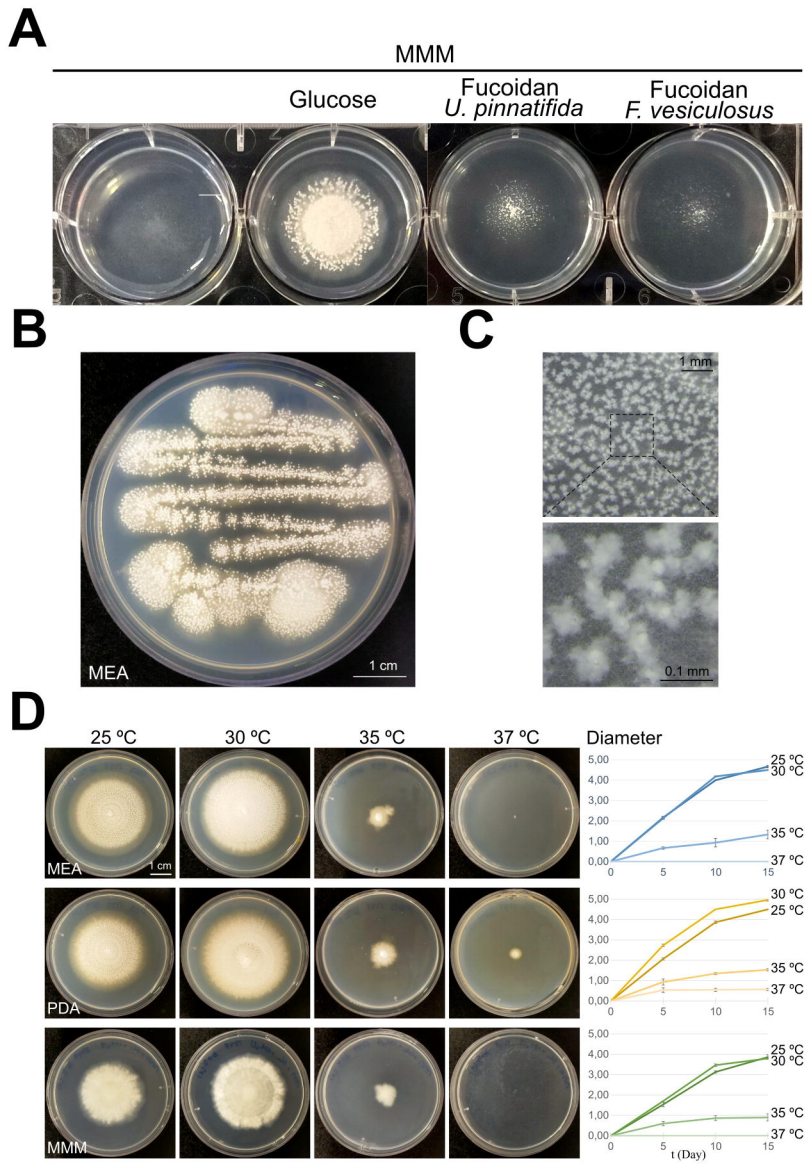
A
MMM
Glucose
Fucoidan
U. pinnatifida
Fucoidan
F. vesiculosus
B
MEA
1 cm
C
1 mm
0.1 mm
D
25 ºC
30 ºC
35 ºC
37 ºC
Diameter
MEA
1 cm
PDA
MMM
25 ºC
30 ºC
35 ºC
37 ºC
t (Day)

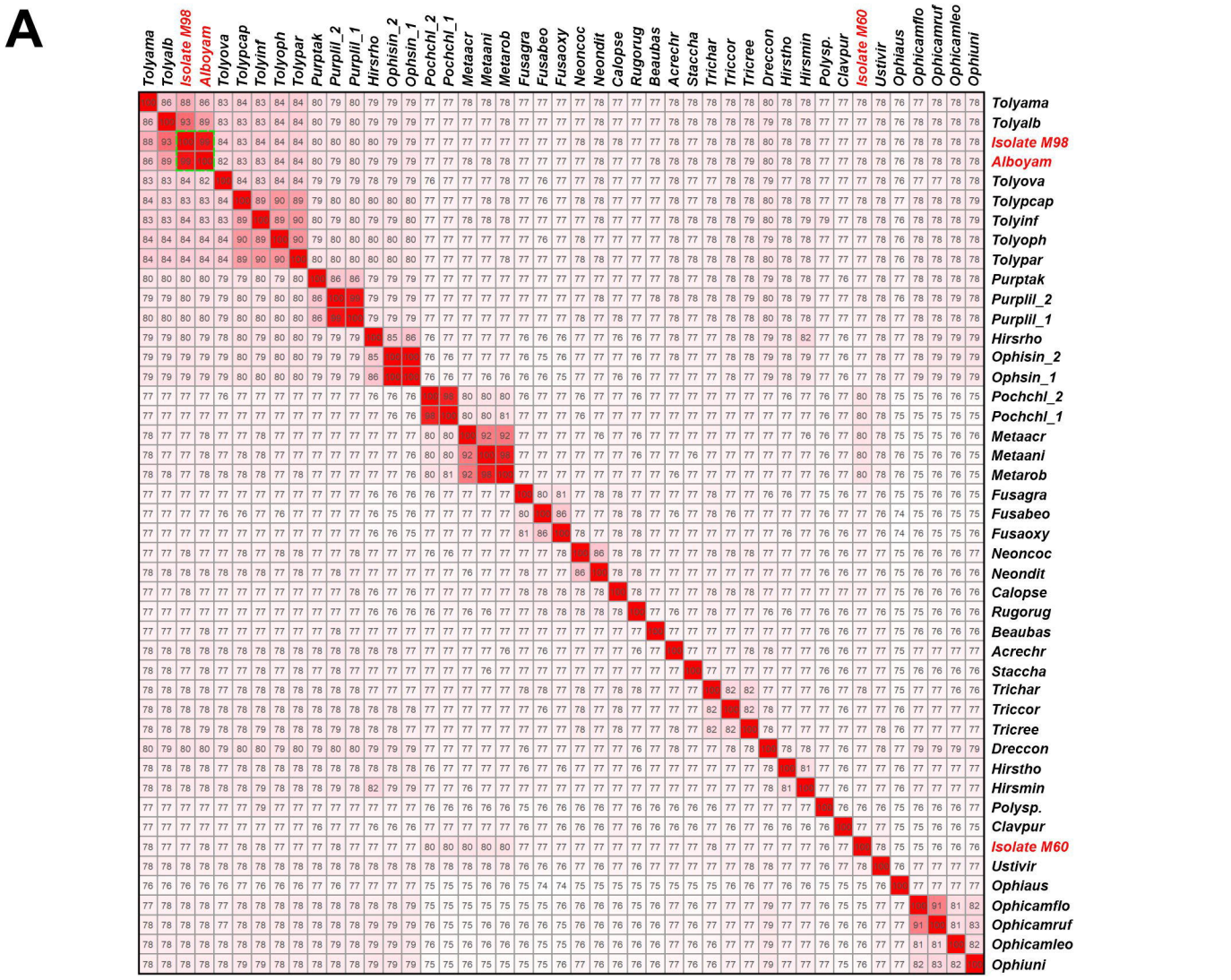
A
Tolyama
Tolyalb
Isolate M98
Alboyam
Tolyova
Tolypcap
Tolyinf
Tolyoph
Tolypar
Purptak
Purplil_2
Purplil_1
Hirsrho
Ophisin_2
Ophsin_1
Pochchl_2
Pochchl_1
Metaacr
Metaani
Metarob
Fusagra
Fusabeo
Fusaoxy
Neoncoc
Neondit
Calopse
Rugorug
Beaubas
Acrechr
Staccha
Trichar
Triccor
Tricree
Dreccon
Hirstho
Hirsmin
Polysp.
Clavpur
Isolate M60
Ustivir
Ophiaus
Ophicamflo
Ophicamruf
Ophicamleo
Ophiuni

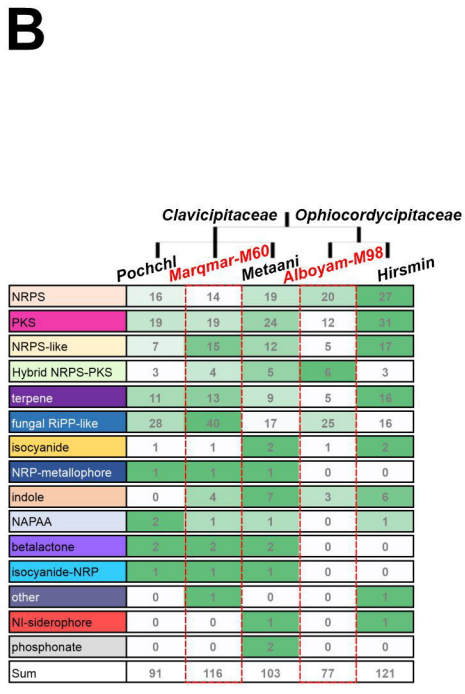
B
Clavicipitaceae
Ophiocordycipitaceae
Pochchl
Marqmar-M60
Metaani
Alboyam-M98
Hirsmin
NRPS 16 14 19 20 27
PKS 19 19 24 12 31
NRPS-like 7 15 12 5 17
Hybrid NRPS-PKS 3 4 5 6 3
terpene 11 13 9 5 16
fungal RiPP-like 28 40 17 25 16
isocyanide 1 1 2 1 2
NRP-metallophore 1 1 1 0 0
indole 0 4 7 3 6
NAPAA 2 1 1 0 1
betalactone 2 2 2 0 0
isocyanide-NRP 1 1 1 0 0
other 0 1 0 0 1
NI-siderophore 0 0 1 0 1
phosphonate 0 0 2 0 0
Sum 91 116 103 77 121

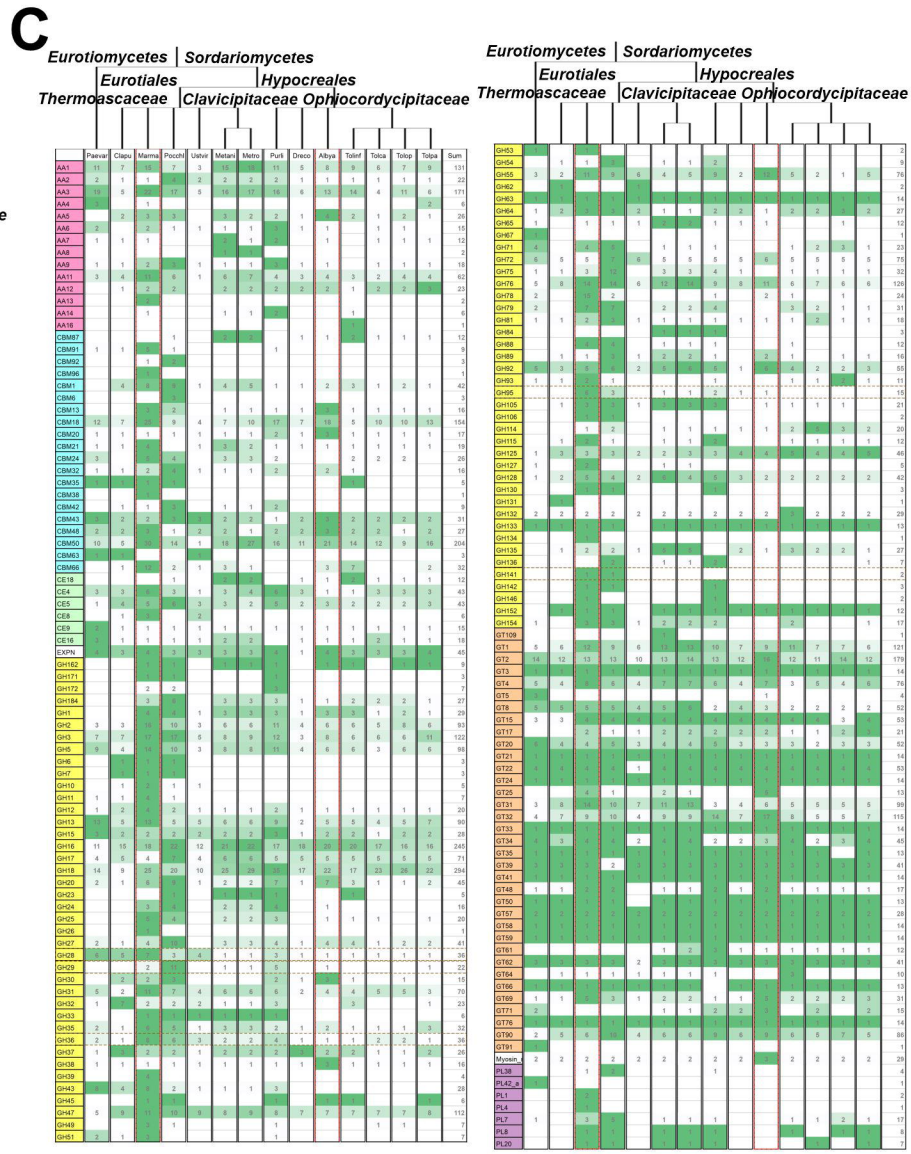
C
Eurotiomycetes
Sordariomycetes
Eurotiales
Hypocreales
Thermoascaceae
Clavicipitaceae
Ophiocordycipitaceae

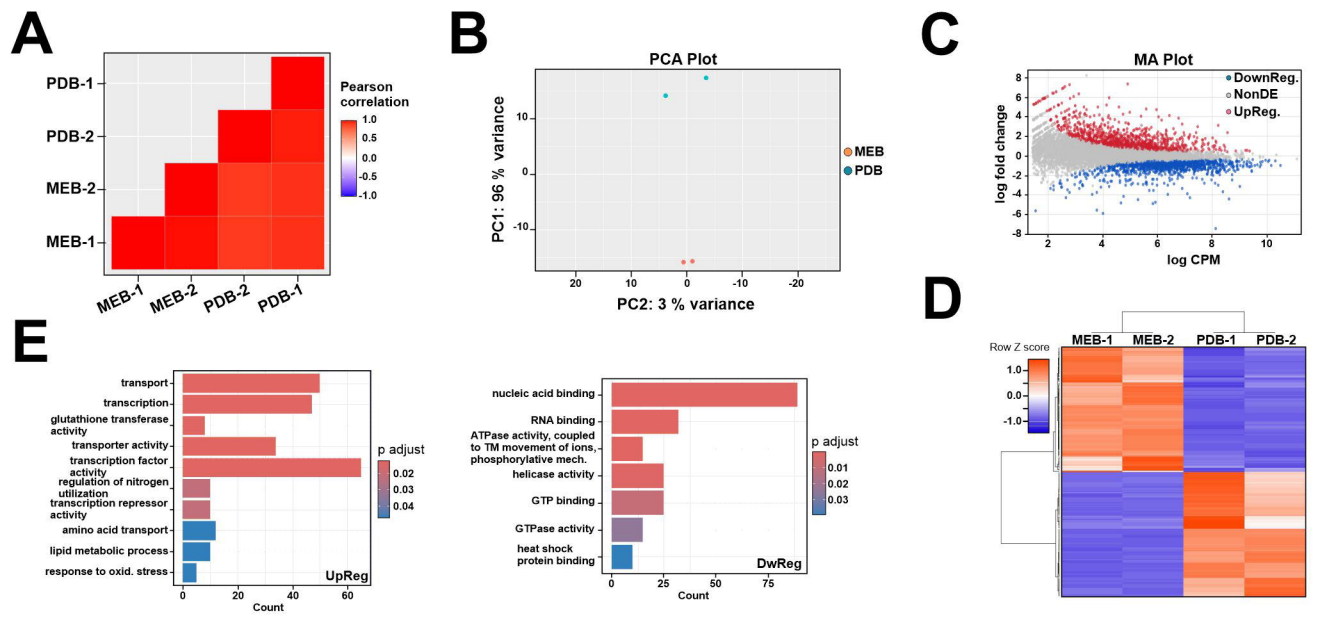

F

		mRNA	Value MEB	Value PDB	log2FC	Interpro	Interpro	L (aa)
Top20 UpReg	1	mRNA_4002	1,7	268,7	7,33	Glutathione transferase family	IPR040079	217
	2	mRNA_8421	0,2	31,1	7,25	Glutathione transferase family	IPR040079	228
	3	mRNA_4091	0,2	26,1	7,07	None predicted	None predicted	329
	4	mRNA_10373	0,2	24,7	6,92	Short-chain dehydrogenase/reductase SDR	IPR002347	270
	5	mRNA_1943	0,2	23,4	6,86	Phosphoenolpyruvate synthase	IPR006319	784
	6	mRNA_690	0,6	43,6	6,31	Aldehyde Dehydrogenase Superfamily	IPR050740	482
	7	mRNA_7372	0,6	36,3	6,03	None predicted	None predicted	275
	8	mRNA_5950	2,2	134,8	5,91	Protein of unknown function DUF1993	IPR018531	172
	9	mRNA_5266	0,6	31,4	5,83	Polyketide synthase, enoylreductase domain	IPR020843	354
	10	mRNA_5136	0,5	22,9	5,38	Aldehyde dehydrogenase domain	IPR015590	503
	11	mRNA_10151	0,5	20,1	5,20	Glycosyl Hydrolase Family 31	IPR051816	633
	12	mRNA_8744	0,5	19,7	5,20	Major facilitator superfamily	IPR011701	453
	13	mRNA_4961	3,3	120,1	5,17	None predicted	None predicted	247
	14	mRNA_5966	0,6	19,9	5,17	Acetylcholinesterase-related enzymes	IPR050654	572
	15	mRNA_11681	1,1	38,0	5,11	FAD-dependent oxidoreductase	IPR050260	546
	16	mRNA_6770	2,7	86,8	4,99	Rifampicin monooxygenase-like	IPR050641	590
	17	mRNA_1398	6,1	189,2	4,96	Phytase-like domain	IPR027372	515
	18	mRNA_5606	1,7	51,6	4,94	Elongation Factors and Glutathione S-transferases	IPR050802	228
	19	mRNA_6513	19,0	509,9	4,74	Major facilitator superfamily	IPR011701	617
	20	mRNA_5983	1,1	29,4	4,74	NmrA-like oxidoreductase	IPR051164	305
Top20 DwReg	1	mRNA_11689	6661,1	38,4	-7,44	RTA-like protein	IPR007568	290
	2	mRNA_1926	107,9	1,8	-5,94	None predicted	None predicted	103
	3	mRNA_2606	84,4	1,8	-5,55	Zinc Chaperone and cDPG Synthetase	IPR051927	614
	4	mRNA_423	664,2	22,3	-4,90	L-aspartate N-monooxygenase (nitrosuccinate-forming)	IPR052189	663
	5	mRNA_7681	205,5	7,3	-4,82	D-1-pyrroline-5-carboxylate dehydrogenase	IPR005931	581
	6	mRNA_4784	721,1	26,8	-4,75	Amino acid adenylation domain	IPR010071	1666
	7	mRNA_4363	378,5	16,7	-4,51	AMP-dependent synthetase/ligase domain	IPR000873	671
	8	mRNA_903	10460,4	476,3	-4,46	Lipoxygenase	IPR000907	711
	9	mRNA_4683	26,1	1,3	-4,31	None predicted	None predicted	108
	10	mRNA_1870	2522,2	128,2	-4,30	ICL/PEPM domain	IPR039556	351
	11	mRNA_77	221,9	12,0	-4,20	MTOX family	IPR045170	498
	12	mRNA_5540	1095,6	69,2	-3,99	Protein of unknown function DUF1275	IPR010699	265
	13	mRNA_1451	68,0	4,4	-3,94	None predicted	None predicted	230
	14	mRNA_12230	2252,1	148,9	-3,92	Serine protease/Carboxylesterase S33	IPR051601	532
	15	mRNA_2685	80,3	5,9	-3,76	Major facilitator superfamily	IPR011701	511
	16	mRNA_4631	29,5	2,2	-3,74	Immunoregulatory Receptor-like	IPR051694	282
	17	mRNA_7739	8091,8	621,8	-3,70	P-type ATPase, subfamily IIIB	IPR006415	937
	18	mRNA_12038	545,5	46,3	-3,56	FAD-dependent monooxygenase	IPR051104	460
	19	mRNA_9511	640,1	54,6	-3,55	Cysteine synthase/Cystathionine beta-synthase	IPR050214	528
	20	mRNA_9868	26,5	2,3	-3,51	None predicted	None predicted	360

G

Cluster	# genes	ratio
c1.1	18	0,17
c1.2	3	0,33
c1.3	12	0,58
c1.4	7	0,29
c1.5	24	0,17
c1.6	18	0,33
c1.7	13	0,15
c1.8	13	0,00
c1.9	27	0,15
c1.10	8	0,25
c1.11	22	0,05
c1.12	14	0,00
c2.1	19	0,37
c2.2	13	0,15
c2.3	10	0,10
c2.4	17	0,18
c2.5	9	0,33
c2,6	20	0,25
c3.1	13	0,15
c3.2	13	0,23
c3.3	12	0,33
c4.1	10	0,20
c4.2	14	0,00
c4.3	13	0,31
c4.4	10	0,30
c4.5	15	0,13
c4.6	10	0,20
c4.7	17	0,00
c4.8	10	0,10
c5.1	16	0,19
c5.2	14	0,14
c5.3	32	0,16
c6.1	16	0,13
c6.2	18	0,06
c6.3	6	0,00
c6.4	18	0,17
c6.5	16	0,69
c6.6	10	0,30
c6.7	9	0,22
c7.1	21	0,14
c7.2	23	0,13
c8.1	24	0,08
c8.2	22	0,27
c8.3	23	0,04
c9.1	13	0,23
c9.2	20	0,10
c9.3	21	0,19
c9.4	25	0,32
c9.5	5	0,40
c9.6	23	0,13
c9.7	17	0,24
c11.1	14	0,07
c11.2	11	0,27
c11.3	6	0,00
c11.4	15	0,20
c12.1	9	0,33
c13.1	15	0,20
c13.2	28	0,07
c13.3	16	0,13
c14.1	15	0,13
c15.1	5	0,40
c16.1	14	0,21
c16.2	6	0,17
c16.3	18	0,11
c16.4	17	0,06
c16.5	28	0,36
c18.1	26	0,04
c19.1	24	0,29
c20.1	7	0,29
c21.1	20	0,10
c21.2	13	0,15
c23.1	23	0,00
c23.2	7	0,29
c25.1	12	0,08
c27.1	8	0,38
c29.1	14	0,36
c29.2	10	0,20
c30.1	4	0,25
c35.1	7	0,00
c36.1	17	0,12
c41.1	19	0,05
c51.1	5	0,00
c53.1	5	0,40
c56.1	6	0,50

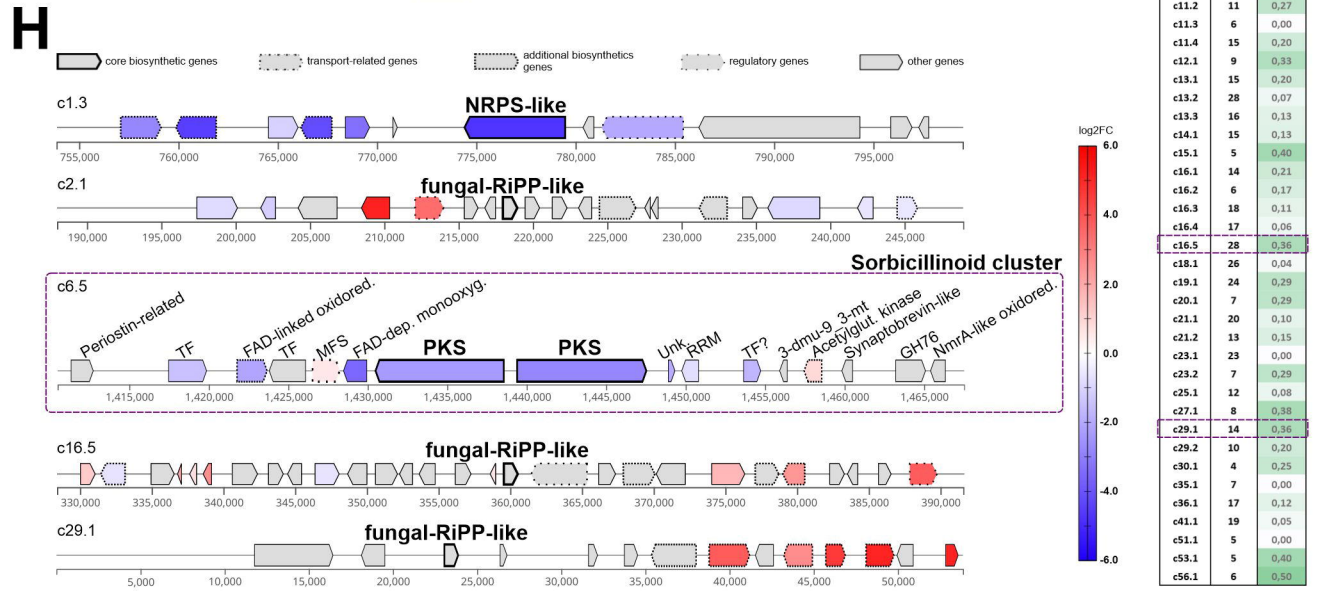

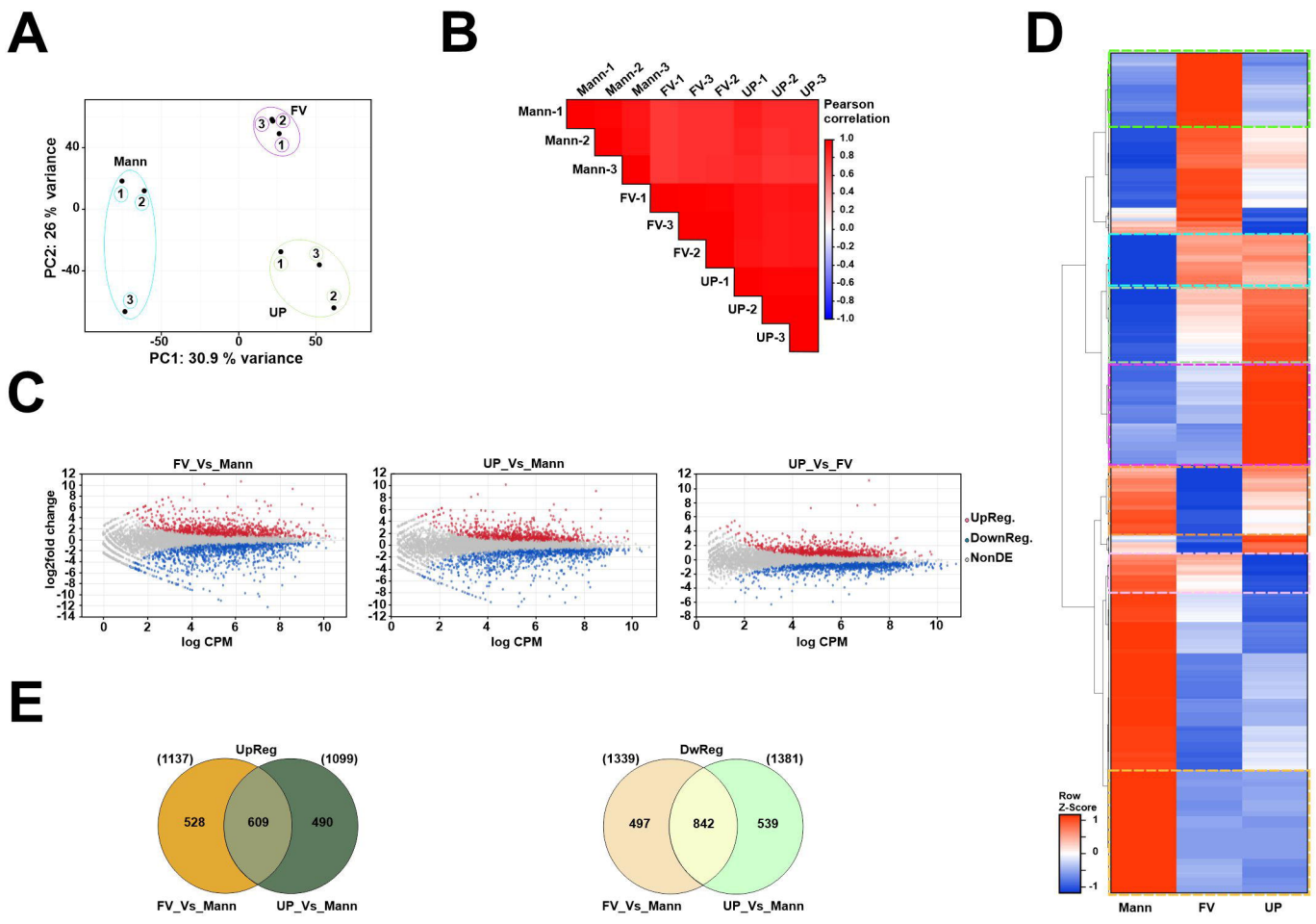
A
Mann
FV
UP
PC2: 26 % variance
PC1: 30.9 % variance
B
Mann-1
Mann-2
Mann-3
FV-1
FV-3
FV-2
UP-1
UP-2
UP-3
Pearson correlation
C
FV_Vs_Mann
UP_Vs_Mann
UP_Vs_FV
log2fold change
log CPM
UpReg.
DownReg.
NonDE
D
Row Z-Score
Mann
FV
UP
E
UpReg
(1137)
(1099)
528
609
490
FV_Vs_Mann
UP_Vs_Mann
DwReg
(1339)
(1381)
497
842
539
FV_Vs_Mann
UP_Vs_Mann

FV_Vs_Mann

mRNA	Value Mann	Value FV	log2FC	Interpro	Interpro	L (aa)
mRNA_4739	0,6	1005,9	10,68	DUF7029	IPR054293	469
mRNA_8581	0,2	188,5	10,12	None predicted	None predicted	304
mRNA_6458	17,0	10499,9	9,27	P-type ATPase	IPR001757	1117
mRNA_7353	2,3	548,8	7,91	RTA-like protein	IPR007568	298
mRNA_9550	0,3	72,6	7,76	D-isomer specific 2-hydroxyacid dehydrogenase	PF02826	352
mRNA_735	0,2	36,4	7,75	Secreted thaumatin-like protein cetA-like	IPR006771	161
mRNA_2611	0,2	27,0	7,31	None predicted	None predicted	271
mRNA_5369	0,2	27,4	7,31	None predicted	None predicted	211
mRNA_7937	0,6	96,0	7,22	Cytochrome P450 monooxygenase	IPR050121	535
mRNA_3670	14,1	2004,9	7,15	None predicted	None predicted	169
mRNA_2881	0,3	41,5	7,00	Amidase	PF01425	528
mRNA_3488	23,6	2906,4	6,94	Major facilitator superfamily	IPR011701	521
mRNA_1791	0,2	20,4	6,87	A_NRPS	cd05930	1832
mRNA_1839	183,5	15728,2	6,42	Glycoside hydrolase, family 76	IPR005198	477
mRNA_6303	0,3	27,9	6,38	Mycotoxin biosynthesis protein UstYa-like	IPR021765	229
mRNA_7490	51,1	3893,1	6,25	Amino Acid-Polyamine-Organocation Superfamily YAT	IPR050524	577
mRNA_6270	45,6	3388,2	6,22	None predicted	None predicted	986
mRNA_428	0,6	44,6	6,20	RTA-like protein	IPR007568	294
mRNA_3001	0,3	23,2	6,08	DUF6987	PF22485	1074
mRNA_382	13,7	867,1	5,99	None predicted	None predicted	449

mRNA	Value Mann	Value FV	log2FC	Interpro	Interpro	L (aa)
mRNA_6307	3388,7	0,7	-12,22	None predicted	None predicted	119
mRNA_3101	405,6	0,2	-11,06	Tripeptidyl-peptidase I and related peptidases	IPR050819	625
mRNA_3764	358,6	0,2	-10,88	Tripeptidyl-peptidase I and related peptidases	IPR050819	522
mRNA_7629	2287,1	1,8	-10,34	Oligopeptide transporter, OPT superfamily	IPR004813	819
mRNA_2012	2167,9	2,4	-9,79	Major facilitator superfamily	IPR011701	493
mRNA_1089	1205,8	1,4	-9,75	Oligopeptide transporter, OPT superfamily	IPR004813	917
mRNA_7888	241,4	0,4	-9,33	HPP	IPR007065	310
mRNA_8717	108,0	0,2	-9,17	None predicted	None predicted	139
mRNA_9199	98,1	0,2	-9,02	Phytanoyl-CoA dioxygenase-like	IPR008775	270
mRNA_8145	181,6	0,4	-8,94	DUF7605	IPR056024	915
mRNA_7574	88,8	0,2	-8,90	Major facilitator superfamily	IPR011701	589
mRNA_4303	79,4	0,2	-8,70	Cytochrome P450 monooxygenase	IPR050121	453
mRNA_3171	445,4	1,4	-8,32	Phospholipase D-like domain	IPR025202	629
mRNA_2315	6518,0	20,7	-8,30	None predicted	None predicted	184
mRNA_8790	56,4	0,2	-8,20	None predicted	None predicted	202
mRNA_6852	52,3	0,2	-8,16	Polygalacturonase QRT3-like	IPR039279	1435
mRNA_7027	56,9	0,2	-8,13	DUF7709	IPR056126	108
mRNA_6018	98,7	0,4	-8,04	Aldo/Keto Reductase	IPR050791	331
mRNA_6743	96,9	0,4	-8,02	Zeta Carotene Desaturase and Related Oxidoreductases	IPR050464	469
mRNA_2263	51,6	0,2	-7,97	None predicted	None predicted	117

UP_Vs_Mann

mRNA	Value Mann	Value UP	log2FC	Interpro	Interpro	L (aa)
mRNA_8581	0,2	229,5	10,13	None predicted	None predicted	304
mRNA_6458	18,2	9726,2	9,06	P-type ATPase	IPR001757	1117
mRNA_1791	0,2	70,6	8,48	A_NRPS	cd05930	1832
mRNA_735	0,2	53,4	8,02	Secreted thaumatin-like protein cetA-like	IPR006771	161
mRNA_9953	14,9	1687,9	6,82	ABC-transporter-regulating transcription factor-like	IPR050987	609
mRNA_9405	47,0	2746,3	5,87	Sulfatase	PF00884	512
mRNA_1839	200,3	11711,2	5,87	Glycoside hydrolase, family 76	IPR005198	477
mRNA_3920	1,4	81,0	5,84	Cyt_b561_FRRS1_like	cd08760	213
mRNA_4770	0,4	22,2	5,83	Coagulation factors 5/8 type C domain (FA58C) profile	IPR000421	267
mRNA_4739	0,7	39,9	5,80	DUF7029	IPR054293	469
mRNA_3488	25,4	1392,2	5,78	Major facilitator superfamily	IPR011701	521
mRNA_2586	1,8	95,1	5,75	Syntaxin	IPR045242	241
mRNA_8750	2,8	131,9	5,55	DUF1254 - DUF1214	IPR010621	331
mRNA_5672	7,6	323,4	5,41	DUF4396	PF14342	213
mRNA_6297	7,1	251,4	5,14	None predicted	None predicted	245
mRNA_6176	2,1	65,7	4,96	Multicopper oxidase, fungi	IPR017762	598
mRNA_7374	1,4	42,4	4,91	None predicted	None predicted	215
mRNA_9129	48,8	1458,1	4,90	Proton-dependent oligopeptide transporter family	IPR000109	613
mRNA_428	0,7	21,5	4,90	RTA-like protein	IPR007568	294
mRNA_7490	57,1	1604,5	4,81	Amino Acid-Polyamine-Organocation Superfamily YAT	IPR050524	577

mRNA	Value Mann	Value UP	log2FC	Interpro	Interpro	L (aa)
mRNA_7858	388,3	0,3	-10,27	None predicted	None predicted	135
mRNA_7629	2679,3	3,3	-9,67	Oligopeptide transporter, OPT superfamily	IPR004813	819
mRNA_6858	122,4	0,2	-9,62	None predicted	None predicted	107
mRNA_3101	446,1	0,6	-9,47	Tripeptidyl-peptidase I and related peptidases	IPR050819	625
mRNA_7574	97,1	0,2	-9,16	Major facilitator superfamily	IPR011701	589
mRNA_3171	495,9	0,9	-9,06	Phospholipase D-like domain	IPR025202	629
mRNA_9724	79,4	0,2	-8,88	Trichothecene Biosynthesis Acetyltransferases	IPR052523	251
mRNA_6307	4111,8	9,3	-8,79	None predicted	None predicted	119
mRNA_2263	65,1	0,2	-8,65	None predicted	None predicted	117
mRNA_1089	1408,1	3,7	-8,57	Oligopeptide transporter, OPT superfamily	IPR004813	917
mRNA_6852	56,3	0,2	-8,38	Polygalacturonase QRT3-like	IPR039279	1435
mRNA_7151	49,1	0,2	-8,20	GmrSD restriction endonucleases, C-terminal domain	IPR011089	207
mRNA_2249	45,8	0,2	-8,15	None predicted	None predicted	148
mRNA_3764	406,2	1,5	-8,08	Tripeptidyl-peptidase I and related peptidases	IPR050819	522
mRNA_4303	88,4	0,3	-8,06	Cytochrome P450 monooxygenase	IPR050121	453
mRNA_4029	40,8	0,2	-7,93	CFEM domain profile	IPR008427	246
mRNA_4636	36,6	0,2	-7,77	Ferric/Cupric Reductase Transmembrane Component	IPR051410	565
mRNA_8145	202,6	1,2	-7,41	DUF7605	IPR056024	915
mRNA_2012	2472,6	14,6	-7,41	Major facilitator superfamily	IPR011701	493
mRNA_1836	28,6	0,2	-7,40	Aspartic peptidase A1	IPR001461	400

UP_Vs_FV

mRNA	Value FV	Value UP	log2FC	Interpro	Interpro	L (aa)
mRNA_9405	1,2	2626,3	11,14	Sulfatase	PF00884	512
mRNA_4436	16,0	3297,9	7,68	Major facilitator, sugar transporter-like	IPR005828	510
mRNA_9953	8,2	1599,9	7,61	ABC-transporter-regulating transcription factor-like	IPR050987	609
mRNA_7440	1,5	231,9	7,25	Beta-hexosaminidase; GH20	IPR025705	597
mRNA_5644	8,7	159,1	4,19	Choice-of-anchor B domain	TIGR04312	468
mRNA_4536	11,5	175,4	3,93	Indoleamine 2,3-dioxygenase	IPR000898	416
mRNA_5192	1,6	22,6	3,85	Major facilitator superfamily	IPR011701	507
mRNA_7772	87,5	1225,9	3,81	None predicted	None predicted	290
mRNA_184	37,6	505,0	3,75	Cytochrome P450 monooxygenase	IPR050121	519
mRNA_3290	5,3	66,2	3,64	Major facilitator superfamily	IPR011701	639
mRNA_5942	64,6	742,4	3,52	ABC-2 type transporter	IPR013525	1405
mRNA_8413	22,7	245,8	3,44	Phytanoyl-CoA dioxygenase-like	IPR008775	292
mRNA_3384	7,8	80,7	3,37	Bacterial Alkyl/Aryl-Sulfatase	IPR052195	604
mRNA_2174	2,8	28,6	3,35	Flavin-dependent aromatic-ring hydroxylase	IPR051704	426
mRNA_5460	15,5	147,9	3,25	2-oxoadipate dioxygenase/decarboxylase	IPR009770	473
mRNA_9729	9,1	85,2	3,23	Protein kinase domain profile	IPR000719	427
mRNA_4361	117,2	1089,8	3,22	Cytochrome P450 monooxygenase	IPR050121	550
mRNA_4415	25,0	228,7	3,20	Acetoacetyl-CoA synthase	IPR005914	697
mRNA_1243	28,3	258,3	3,19	Cellulose-degrading glycosyl hydrolase 3	IPR050288	761
mRNA_1956	27,7	246,4	3,15	NADH:cytochrome b5 reductase-like	IPR001834	458

mRNA	Value FV	Value UP	log2FC	Interpro	Interpro	L (aa)
mRNA_2881	44,1	0,6	-6,27	Amidase	PF01425	528
mRNA_7353	572,8	9,7	-5,88	RTA-like protein	IPR007568	298
mRNA_4106	23,3	0,6	-5,34	None predicted	None predicted	189
mRNA_6779	65,6	1,7	-5,26	ATP-binding cassette transporter C-like	IPR050173	1390
mRNA_4739	1095,8	37,3	-4,88	DUF7029	IPR054293	469
mRNA_7937	102,2	4,9	-4,39	Cytochrome P450 monooxygenase	IPR050121	535
mRNA_7417	59,0	3,4	-4,11	None predicted	None predicted	588
mRNA_6303	31,7	1,9	-4,07	Mycotoxin biosynthesis protein UstYa-like	IPR021765	229
mRNA_902	26,6	1,6	-4,02	Prolyl 4-hydroxylase	IPR045054	271
mRNA_382	890,0	59,2	-3,91	None predicted	None predicted	449
mRNA_9584	24,6	1,8	-3,75	None predicted	None predicted	151
mRNA_3448	262,7	20,7	-3,67	Nucleobase cation symporter 2 family	IPR006043	598
mRNA_3711	535,4	44,2	-3,60	Zn2/Cys6 DNA-binding domain	SSF57701	433
mRNA_10120	169,5	14,7	-3,53	None predicted	None predicted	499
mRNA_1901	103,0	9,2	-3,49	None predicted	None predicted	358
mRNA_3670	2097,0	199,3	-3,40	None predicted	None predicted	169
mRNA_8064	117,6	13,4	-3,13	None predicted	None predicted	155
mRNA_3704	18,6	2,2	-3,06	NSF attachment protein	IPR000744	289
mRNA_2669	417,6	51,8	-3,01	Polyketide and Nonribosomal Peptide Biosynthesis Enz.	IPR05009	2283
mRNA_8416	22,7	3,0	-2,93	Polyketide and Nonribosomal Peptide Biosynthesis Enz.	IPR050091	2578

Top20 UpReg

Top20 DwReg

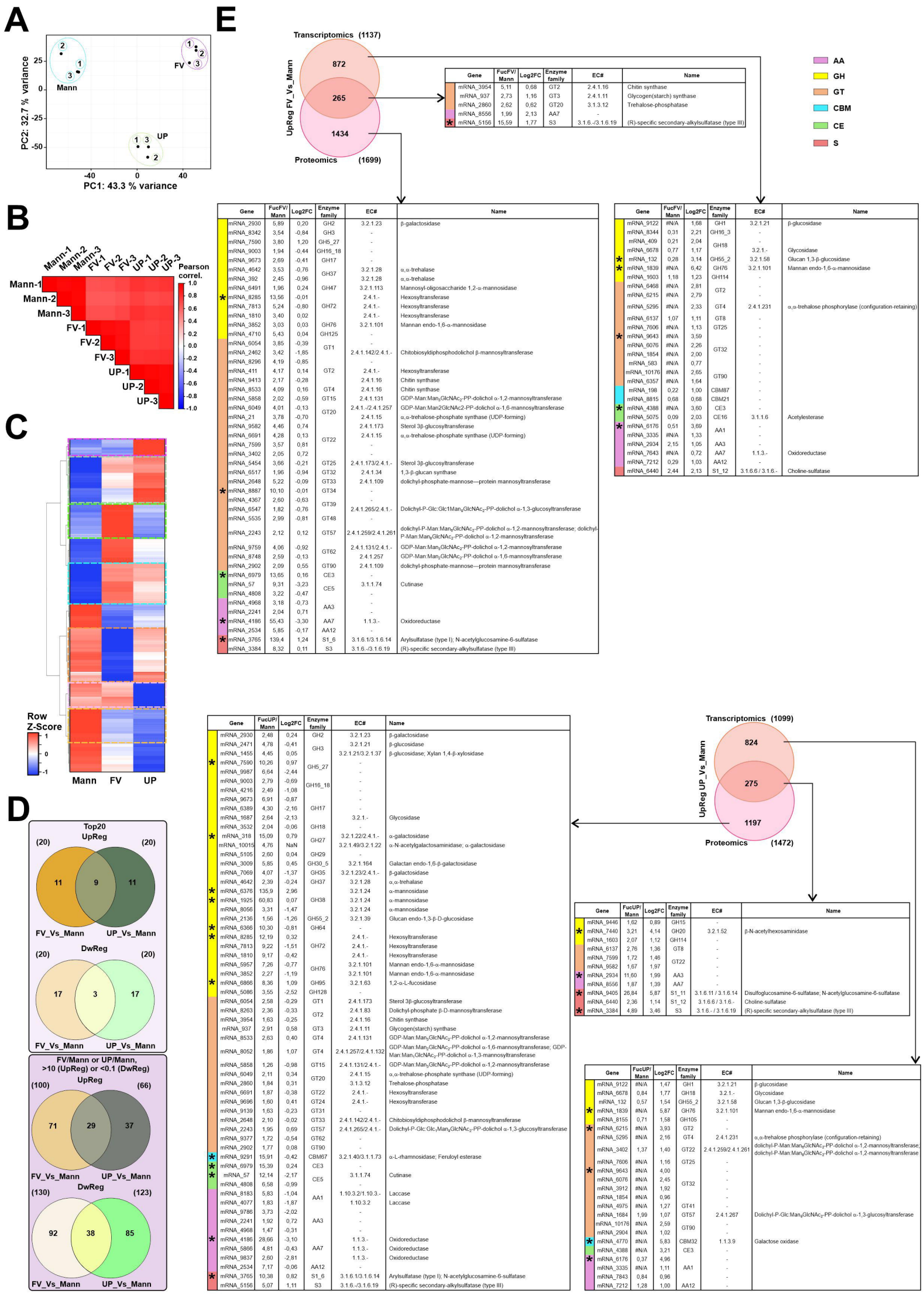

	Gene	FucFV/ Mann	Log2FC	Enzyme family	EC#	Name
	mRNA_3954	5,11	0,68	GT2	2.4.1.16	Chitin synthase
	mRNA_937	2,73	1,16	GT3	2.4.1.11	Glycogen(starch) synthase
	mRNA_2860	2,62	0,62	GT20	3.1.3.12	Trehalose-phosphatase
	mRNA_8556	1,99	2,13	AA7	-	
*	mRNA_5156	15,59	1,77	S3	3.1.6.-/3.1.6.19	(R)-specific secondary-alkylsulfatase (type III)

	Gene	FucFV/ Mann	Log2FC	Enzyme family	EC#	Name
	mRNA_2930	5,89	0,20	GH2	3.2.1.23	β-galactosidase
	mRNA_8342	3,54	-0,84	GH3	-	
	mRNA_7590	3,80	1,20	GH5_27	-	
	mRNA_9003	1,94	-0,44	GH16_18	-	
	mRNA_9673	2,69	-0,41	GH17	-	
	mRNA_4642	3,53	-0,76	GH37	3.2.1.28	α,α-trehalase
	mRNA_392	2,45	-0,96		3.2.1.28	α,α-trehalase
	mRNA_6491	1,96	0,24	GH47	3.2.1.113	Mannosyl-oligosaccharide 1,2-α-mannosidase
*	mRNA_8285	13,56	-0,01	GH72	2.4.1.-	Hexosyltransferase
	mRNA_7813	5,24	-0,80		2.4.1.-	Hexosyltransferase
	mRNA_1810	3,40	0,02		2.4.1.-	Hexosyltransferase
	mRNA_3852	3,03	0,03	GH76	3.2.1.101	Mannan endo-1,6-α-mannosidase
	mRNA_4710	5,43	0,04	GH125	-	
	mRNA_6054	3,85	-0,39	GT1	-	
	mRNA_2462	3,42	-1,85		2.4.1.142/2.4.1.-	Chitobiosyldiphosphodolichol β-mannosyltransferase
	mRNA_8296	4,19	-0,85		-	
	mRNA_411	4,17	0,14	GT2	2.4.1.-	Hexosyltransferase
	mRNA_9413	2,17	-0,28		2.4.1.16	Chitin synthase
	mRNA_8533	4,09	0,16	GT4	2.4.1.16	Chitin synthase
	mRNA_5858	2,02	-0,59	GT15	2.4.1.131	GDP-Man:$Man_3GlcNAc_2$-PP-dolichol α-1,2-mannosyltransferase
	mRNA_6049	4,01	-0,13	GT20	2.4.1.-/2.4.1.257	GDP-Man:Man2GlcNAc2-PP-dolichol α-1,6-mannosyltransferase
	mRNA_21	3,78	-0,70		2.4.1.15	α,α-trehalose-phosphate synthase (UDP-forming)
	mRNA_9582	4,46	0,74		2.4.1.173	Sterol 3β-glucosyltransferase
	mRNA_6691	4,28	0,13	GT22	2.4.1.15	α,α-trehalose-phosphate synthase (UDP-forming)
	mRNA_7599	3,57	0,81		-	
	mRNA_3402	2,05	0,72		-	
	mRNA_5454	3,66	-0,21	GT25	2.4.1.173/2.4.1.-	Sterol 3β-glucosyltransferase
	mRNA_6517	1,96	-0,94	GT32	2.4.1.34	1,3-β-glucan synthase
	mRNA_2648	5,22	-0,09	GT33	2.4.1.109	dolichyl-phosphate-mannose—protein mannosyltransferase
*	mRNA_8887	10,10	-0,01	GT34	-	
	mRNA_4367	2,60	-0,63	GT39	-	
	mRNA_6547	1,82	-0,76		2.4.1.265/2.4.1.-	Dolichyl-P-Glc:Glc1$Man_9GlcNAc_2$-PP-dolichol α-1,3-glucosyltransferase
	mRNA_5535	2,99	-0,81	GT48	-	
	mRNA_2243	2,12	0,12	GT57	2.4.1.259/2.4.1.261	dolichyl-P-Man:$Man_9GlcNAc_2$-PP-dolichol α-1,2-mannosyltransferase; dolichyl-P-Man:$Man_8GlcNAc_2$-PP-dolichol α-1,2-mannosyltransferase
	mRNA_9759	4,06	-0,92	GT62	2.4.1.131/2.4.1.-	GDP-Man:$Man_3GlcNAc_2$-PP-dolichol α-1,2-mannosyltransferase
	mRNA_8748	2,59	-0,13		2.4.1.257	GDP-Man:$Man_5GlcNAc_2$-PP-dolichol α-1,6-mannosyltransferase
	mRNA_2902	2,09	0,55	GT90	2.4.1.109	dolichyl-phosphate-mannose—protein mannosyltransferase
*	mRNA_6979	13,65	0,16	CE3	-	
	mRNA_57	9,31	-3,23	CE5	3.1.1.74	Cutinase
	mRNA_4808	3,22	-0,47		-	
	mRNA_4968	3,18	-0,73	AA3	-	
	mRNA_2241	2,04	0,71		-	
*	mRNA_4186	55,43	-3,30	AA7	1.1.3.-	Oxidoreductase
	mRNA_2534	5,85	-0,17	AA12	-	
*	mRNA_3765	139,4	1,24	S1_6	3.1.6.1/3.1.6.14	Arylsulfatase (type I); N-acetylglucosamine-6-sulfatase
	mRNA_3384	8,32	0,11	S3	3.1.6.-/3.1.6.19	(R)-specific secondary-alkylsulfatase (type III)

	Gene	FucFV/ Mann	Log2FC	Enzyme family	EC#	Name
	mRNA_9122	#N/A	1,68	GH1	3.2.1.21	β-glucosidase
	mRNA_8344	0,31	2,21	GH16_3	-	
	mRNA_409	0,21	2,04	GH18	-	
	mRNA_6678	0,77	1,17		3.2.1.-	Glycosidase
*	mRNA_132	0,28	3,14	GH55_2	3.2.1.58	Glucan 1,3-β-glucosidase
*	mRNA_1839	#N/A	6,42	GH76	3.2.1.101	Mannan endo-1,6-α-mannosidase
	mRNA_1603	1,18	1,23	GH114	-	
	mRNA_6468	#N/A	2,81	GT2	-	
	mRNA_6215	#N/A	2,79		-	
	mRNA_5295	#N/A	2,33	GT4	2.4.1.231	α,α-trehalose phosphorylase (configuration-retaining)
	mRNA_6137	1,07	1,11	GT8	-	
	mRNA_7606	#N/A	1,13	GT25	-	
*	mRNA_9643	#N/A	3,59	GT32	-	
	mRNA_6076	#N/A	2,26		-	
	mRNA_1854	#N/A	2,00		-	
	mRNA_583	#N/A	0,77		-	
	mRNA_10176	#N/A	2,65	GT90	-	
	mRNA_6357	#N/A	1,64		-	
	mRNA_198	0,22	1,00	CBM87	-	
	mRNA_8815	0,68	0,68	CBM21	-	
*	mRNA_4388	#N/A	3,60	CE3	-	
	mRNA_5075	0,09	2,03	CE16	3.1.1.6	Acetylesterase
*	mRNA_6176	0,51	3,69	AA1	-	
	mRNA_3335	#N/A	1,33		-	
	mRNA_2934	2,15	1,05	AA3	-	
	mRNA_7643	#N/A	0,72	AA7	1.1.3.-	Oxidoreductase
	mRNA_7212	0,29	1,03	AA12	-	
	mRNA_6440	2,44	2,13	S1_12	3.1.6.6 / 3.1.6.-	Choline-sulfatase

	Gene	FucUP/ Mann	Log2FC	Enzyme family	EC#	Name
	mRNA_2930	2,48	0,24	GH2	3.2.1.23	β-galactosidase
	mRNA_2471	4,78	-0,41	GH3	3.2.1.21	β-glucosidase
	mRNA_1455	4,45	0,05		3.2.1.21/3.2.1.37	β-glucosidase; Xylan 1,4-β-xylosidase
*	mRNA_7590	10,26	0,97	GH5_27	-	
	mRNA_9987	6,64	-2,44		-	
	mRNA_9003	2,79	-0,69	GH16_18	-	
	mRNA_4216	2,49	-1,08		-	
	mRNA_9673	6,91	-0,87		-	
	mRNA_6389	4,30	-2,16	GH17	-	
	mRNA_1687	2,64	-2,13		3.2.1.-	Glycosidase
	mRNA_3532	2,04	-0,06	GH18	-	
*	mRNA_318	15,09	0,79	GH27	3.2.1.22/2.4.1.-	α-galactosidase
	mRNA_10015	4,76	NaN		3.2.1.49/3.2.1.22	α-N-acetylgalactosaminidase; α-galactosidase
	mRNA_5105	2,60	0,04	GH29	-	
	mRNA_3009	5,85	0,45	GH30_5	3.2.1.164	Galactan endo-1,6-β-galactosidase
	mRNA_7069	4,07	-1,37	GH35	3.2.1.23/2.4.1.-	β-galactosidase
	mRNA_4642	2,39	-0,24	GH37	3.2.1.28	α,α-trehalase
*	mRNA_6376	135,9	2,96		3.2.1.24	α-mannosidase
*	mRNA_1925	60,83	0,07	GH38	3.2.1.24	α-mannosidase
	mRNA_8056	3,31	-1,47		3.2.1.24	α-mannosidase
	mRNA_2136	1,56	-1,26	GH55_2	3.2.1.39	Glucan endo-1,3-β-D-glucosidase
*	mRNA_6366	10,30	-0,81	GH64	-	
*	mRNA_8285	12,19	0,32		2.4.1.-	Hexosyltransferase
	mRNA_7813	9,22	-1,51	GH72	2.4.1.-	Hexosyltransferase
	mRNA_1810	9,17	-0,42		2.4.1.-	Hexosyltransferase
	mRNA_5957	7,26	-0,77	GH76	3.2.1.101	Mannan endo-1,6-α-mannosidase
	mRNA_3852	2,27	-1,19		3.2.1.101	Mannan endo-1,6-α-mannosidase
*	mRNA_6866	8,36	1,09	GH95	3.2.1.63	1,2-α-L-fucosidase
	mRNA_5086	3,55	-2,52	GH128	-	
	mRNA_6054	2,58	-0,29	GT1	2.4.1.173	Sterol 3β-glucosyltransferase
	mRNA_8263	2,36	-0,33	GT2	2.4.1.83	Dolichyl-phosphate β-D-mannosyltransferase
	mRNA_3954	1,63	-0,25		2.4.1.16	Chitin synthase
	mRNA_937	2,91	0,58	GT3	2.4.1.11	Glycogen(starch) synthase
	mRNA_8533	2,63	0,40	GT4	2.4.1.131	GDP-Man:$Man_3GlcNAc_2$-PP-dolichol α-1,2-mannosyltransferase
	mRNA_8052	1,86	1,07	GT4	2.4.1.257/2.4.1.132	GDP-Man:$Man_5GlcNAc_2$-PP-dolichol α-1,6-mannosyltransferase; GDP-Man:$Man_3GlcNAc_2$-PP-dolichol α-1,3-mannosyltransferase
	mRNA_5858	1,26	-0,98	GT15	2.4.1.131/2.4.1.-	GDP-Man:$Man_3GlcNAc_2$-PP-dolichol α-1,2-mannosyltransferase
	mRNA_6049	2,11	0,34	GT20	2.4.1.15	α,α-trehalose-phosphate synthase (UDP-forming)
	mRNA_2860	1,84	0,31		3.1.3.12	Trehalose-phosphatase
	mRNA_6691	1,87	-0,38	GT22	2.4.1.-	Hexosyltransferase
	mRNA_9696	1,60	0,41	GT24	2.4.1.-	Hexosyltransferase
	mRNA_9139	1,63	-0,23	GT31	-	
	mRNA_2648	2,10	-0,02	GT33	2.4.1.142/2.4.1.-	Chitobiosyldiphosphodolichol β-mannosyltransferase
	mRNA_2243	1,95	0,69	GT57	2.4.1.265/2.4.1.-	Dolichyl-P-Glc:$Glc_1Man_9GlcNAc_2$-PP-dolichol α-1,3-glucosyltransferase
	mRNA_9377	1,72	-0,54	GT62	-	
	mRNA_2902	1,77	0,08	GT90	-	
*	mRNA_9291	15,91	-0,42	CBM67	3.2.1.40/3.1.1.73	α-L-rhamnosidase; Feruloyl esterase
*	mRNA_6979	15,39	0,24	CE3	-	
*	mRNA_57	12,14	-2,17	CE5	3.1.1.74	Cutinase
	mRNA_4808	6,58	-0,99		-	
	mRNA_8183	5,83	-1,04	AA1	1.10.3.2/1.10.3.-	Laccase
	mRNA_4077	1,83	-1,87		1.10.3.2	Laccase
	mRNA_9786	3,73	-2,02	AA3	-	
	mRNA_2241	1,92	0,72		-	
	mRNA_4968	1,47	-0,31		-	
*	mRNA_4186	28,66	-3,10	AA7	1.1.3.-	Oxidoreductase
	mRNA_5866	4,81	-0,43		1.1.3.-	Oxidoreductase
	mRNA_9837	2,60	-2,81		1.1.3.-	Oxidoreductase
	mRNA_2534	7,17	-0,06	AA12	-	
*	mRNA_3765	10,38	0,82	S1_6	3.1.6.1/3.1.6.14	Arylsulfatase (type I); N-acetylglucosamine-6-sulfatase
	mRNA_5156	5,07	1,11	S3	3.1.6.-/3.1.6.19	(R)-specific secondary-alkylsulfatase (type III)

	Gene	FucUP/ Mann	Log2FC	Enzyme family	EC#	Name
	mRNA_9446	1,62	0,89	GH15	-	
*	mRNA_7440	3,21	4,14	GH20	3.2.1.52	β-N-acetylhexosaminidase
	mRNA_1603	2,07	1,12	GH114	-	
	mRNA_6137	2,76	1,36	GT8	-	
	mRNA_7599	1,72	1,46	GT22	-	
	mRNA_9582	1,67	1,97		-	
*	mRNA_2934	11,60	1,99	AA3	-	
	mRNA_8556	1,87	1,39	AA7	-	
*	mRNA_9405	26,84	5,87	S1_11	3.1.6.11 / 3.1.6.14	Disulfoglucosamine-6-sulfatase; N-acetylglucosamine-6-sulfatase
	mRNA_6440	2,36	1,14	S1_12	3.1.6.6 / 3.1.6.-	Choline-sulfatase
*	mRNA_3384	4,89	3,46	S3	3.1.6.- / 3.1.6.19	(R)-specific secondary-alkylsulfatase (type III)

	Gene	FucUP/ Mann	Log2FC	Enzyme family	EC#	Name
	mRNA_9122	#N/A	1,47	GH1	3.2.1.21	β-glucosidase
	mRNA_6678	0,84	1,77	GH18	3.2.1.-	Glycosidase
	mRNA_132	0,57	1,54	GH55_2	3.2.1.58	Glucan 1,3-β-glucosidase
*	mRNA_1839	#N/A	5,87	GH76	3.2.1.101	Mannan endo-1,6-α-mannosidase
	mRNA_8155	0,71	1,58	GH105	-	
*	mRNA_6215	#N/A	3,93	GT2	-	
	mRNA_5295	#N/A	2,16	GT4	2.4.1.231	α,α-trehalose phosphorylase (configuration-retaining)
	mRNA_3402	1,37	1,40	GT22	2.4.1.259/2.4.1.261	dolichyl-P-Man:$Man_9GlcNAc_2$-PP-dolichol α-1,2-mannosyltransferase; dolichyl-P-Man:$Man_8GlcNAc_2$-PP-dolichol α-1,2-mannosyltransferase
	mRNA_7606	#N/A	1,16	GT25	-	
*	mRNA_9643	#N/A	4,00	GT32	-	
	mRNA_6076	#N/A	2,45		-	
	mRNA_3912	#N/A	1,92		-	
	mRNA_1854	#N/A	0,96		-	
	mRNA_4975	#N/A	1,27	GT41	-	
	mRNA_1684	1,99	1,07	GT57	2.4.1.267	Dolichyl-P-Glc:$Man_9GlcNAc_2$-PP-dolichol α-1,3-glucosyltransferase
	mRNA_10176	#N/A	2,59	GT90	-	
	mRNA_2904	#N/A	1,02		-	
*	mRNA_4770	#N/A	5,83	CBM32	1.1.3.9	Galactose oxidase
	mRNA_4388	#N/A	3,21	CE3	-	
*	mRNA_6176	0,37	4,96		-	
	mRNA_3335	#N/A	1,11	AA1	-	
	mRNA_7843	0,84	0,96		-	
	mRNA_7212	1,28	1,00	AA12	-	

FV_Vs_Mann

mRNA	Protein	Value Mann	Value FV	FV/Mann	Interpro	Interpro	L (aa)
mRNA_7490	97544	11,0	21,2	1148,15	Amino Acid-Polyamine-Organocation Superfamily YAT	IPR050524	577
mRNA_3765	69959	10,5	17,6	139,41	Arylsulfatase	IPR012083	583
mRNA_1518	94855	13,6	20,1	86,46	None predicted	None predicted	467
mRNA_3058	103800	10,6	17,0	83,70	Mayor Intrinsic Protein (MIP); Aquaporin	IPR000425	337
mRNA_3817	73955	11,0	17,3	74,79	None predicted	None predicted	235
mRNA_2244	81067	10,8	17,0	71,13	Fucose-specific lectin	SSF89372	541
mRNA_2085	96749	10,6	16,5	60,22	S8 peptidase family	IPR015500	419
mRNA_3488	102527	10,7	16,6	59,09	Major Facilitator Superfamily	IPR011701	521
mRNA_4186	100591	10,5	16,3	55,43	FAD-linked Oxidoreductases in Biosynthetic Pathways	IPR050416	474
mRNA_3478	96373	14,9	20,5	49,59	Acid sphingomyelinase/endopolyphosphatase	IPR041805	706
mRNA_5672	93669	10,5	16,1	47,64	None predicted	None predicted	213
mRNA_7420	101195	11,6	17,0	43,37	Amino Acid-Polyamine-Organocation Superfamily YAT	IPR050524	570
mRNA_2835	90910	11,4	16,8	43,34	Fungal Secondary Metabolite SDRs	IPR051468	273
mRNA_2277	99784	10,6	15,9	41,09	CCHC-type Zinc Finger Nucleic Acid Binding	IPR051714	222
mRNA_3283	92468	10,6	15,9	39,45	Oligopeptide transporter (OPT)	IPR004813	903
mRNA_1546	100438	11,8	17,1	38,08	Short-chain dehydrogenase/reductase (SDR)	IPR002347	250
mRNA_6458	104252	12,1	17,3	37,25	P-type ATPase	IPR001757	1117
mRNA_9573	115831	14,6	19,8	36,98	Type-B Carboxylesterase/Lipase	IPR050309	596
mRNA_8938	95313	11,2	16,3	34,11	Phospholipase A2, prokaryotic/fungal	IPR015141	182
mRNA_1015	100914	11,5	16,6	33,79	Claspin	IPR024146	1326

mRNA	Protein	Value Mann	Value FV	FV/Mann	Interpro	Interpro	L (aa)
mRNA_5526	102335	19,4	12,2	0,01	Protein of unknown function DUF4419	IPR025533	440
mRNA_5149	103271	18,7	11,8	0,01	Mitochondrial outer membrane protein OM14	IPR039454	247
mRNA_9070	95791	19,5	12,8	0,01	CFEM domain-containing protein	IPR051735	171
mRNA_8309	96044	18,9	12,3	0,01	ATP synthase, F0 complex, subunit H	IPR019711	130
mRNA_1741	96097	18,3	11,8	0,01	SRP1/TIP1-like Cell Wall Component	IPR052982	249
mRNA_915	96780	18,7	12,6	0,01	Aromatic prenyltransferase	IPR033964	433
mRNA_10099	96554	19,3	13,2	0,01	None predicted	None predicted	155
mRNA_9589	98740	19,1	13,1	0,02	Translation elongation factor IF5A-like	IPR001884	160
mRNA_4245	102326	19,0	13,2	0,02	Histidine phosphatase superfamily	IPR000560	543
mRNA_4569	100736	20,3	14,4	0,02	DUF3759	IPR022234	106
mRNA_3171	96674	17,4	11,7	0,02	Phospholipase D-like domain	IPR025202	629
mRNA_884	73672	20,8	15,1	0,02	Flavin monoamine oxidase and related enzymes	IPR050281	626
mRNA_712	119128	17,4	11,8	0,02	Large ribosomal subunit protein eL30-like	IPR039109	133
mRNA_972	98526	17,0	11,5	0,02	None predicted	None predicted	430
mRNA_3211	102154	17,0	11,6	0,02	Signaling mucin MSB2	IPR039295	723
mRNA_7666	102378	16,6	11,2	0,02	Formyltetrahydrofolate deformylase	IPR004810	286
mRNA_4792	99048	18,6	13,2	0,02	Transcription factor BTF3	IPR039370	156
mRNA_3976	102165	17,1	11,8	0,02	Uncharacterised protein family UPF0145, YbjQ-like	IPR002765	149
mRNA_833	101985	17,2	11,9	0,02	None predicted	None predicted	227
mRNA_2928	75550	16,9	11,6	0,03	Glycoside hydrolase domain, family 65	IPR005195	981

UP_Vs_Mann

mRNA	Protein	Value Mann	Value UP	UP/Mann	Interpro	Interpro	L (aa)
mRNA_6376	97931	12,0	19,1	135,95	Glycoside hydrolase, family 38	IPR000602	1084
mRNA_1518	94855	13,6	20,4	108,21	None predicted	None predicted	467
mRNA_7542	96091	11,8	18,4	97,06	Peptidase, metallopeptidase	IPR006026	275
mRNA_6617	102384	14,0	20,6	94,89	Short-chain dehydrogenase/reductase SDR	IPR002347	260
mRNA_7490	97544	11,0	17,6	93,23	Amino Acid-Polyamine-Organocation Superfamily YAT	IPR050524	577
mRNA_7820	97933	13,3	19,8	90,11	Phytanoyl-CoA dioxygenase-like	IPR008775	274
mRNA_3058	103800	10,6	16,9	80,99	Major Intrinsic Protein (MIP); Aquaporin	IPR050363	337
mRNA_2	99713	10,9	17,2	78,90	Lipase, secreted	IPR005152	458
mRNA_2815	98320	15,3	21,3	63,82	L-rhamnonate dehydratase-like; L-fuconate dehydratase	IPR046945	451
mRNA_1925	104308	11,1	17,1	60,83	Glycoside hydrolase family 38	IPR000602	1084
mRNA_1546	100438	11,8	17,4	48,02	Short-chain dehydrogenase/reductase SDR	IPR002347	250
mRNA_3817	73955	11,0	16,6	46,95	None predicted	None predicted	235
mRNA_3488	102527	10,7	15,7	31,92	Major facilitator superfamily	IPR011701	521
mRNA_7120	94709	10,7	15,7	31,56	None predicted	None predicted	497
mRNA_5738	101184	12,5	17,5	31,29	DapA-like	IPR002220	327
mRNA_7420	101195	11,6	16,5	31,12	Amino Acid-Polyamine-Organocation Superfamily YAT	IPR050524	570
mRNA_661	76888	11,5	16,4	31,10	None predicted	None predicted	320
mRNA_4186	100591	10,5	15,3	28,66	FAD-linked Oxidoreductases in Biosynthetic Pathways	IPR050416	474
mRNA_9405	96484	11,4	16,1	26,84	Sulfatase	PF00884	512
mRNA_3478	96373	14,9	19,6	26,72	Acid sphingomyelinase/ endopolyphosphatase	IPR041805	706

mRNA	Protein	Value Mann	Value UP	UP/Mann	Interpro	Interpro	L (aa)
mRNA_5643	101032	18,2	10,8	0,01	None predicted	None predicted	544
mRNA_256	102832	18,3	11,7	0,01	Nascent polypeptide-associated complex subunit alpha-like	IPR016641	200
mRNA_183	99744	16,7	10,3	0,01	Collagen superfamily	IPR050149	452
mRNA_9223	103250	16,8	10,8	0,02	Aspartic peptidase A1	IPR001461	463
mRNA_9155	101482	16,6	10,6	0,02	Tripeptidyl-peptidase I and related peptidases	IPR050819	681
mRNA_6044	98273	16,9	10,9	0,02	None predicted	None predicted	102
mRNA_5526	102335	19,4	13,8	0,02	Protein of unknown function DUF4419	IPR025533	440
mRNA_4569	100736	20,3	14,7	0,02	Protein of unknown function DUF3759	IPR022234	106
mRNA_4792	99048	18,6	13,1	0,02	Transcription factor BTF3	IPR039370	156
mRNA_1089	102943	16,0	10,6	0,02	Oligopeptide transporter, OPT superfamily	IPR004813	917
mRNA_2249	98046	16,0	10,6	0,02	None predicted	None predicted	148
mRNA_2812	72433	16,2	10,8	0,02	Serine/threonine-protein kinases, AGC	IPR050236	1399
mRNA_5309	89936	16,5	11,2	0,02	Glucanosyltransferase	IPR004886	526
mRNA_4917	89803	18,5	13,1	0,03	Nucleosome assembly protein (NAP)	IPR002164	414
mRNA_5610	86274	16,0	10,7	0,03	Inorganic pyrophosphatase	IPR008162	293
mRNA_4041	117106	16,2	11,0	0,03	Appressorial penetration-associated	IPR053216	554
mRNA_7858	103904	15,8	10,7	0,03	None predicted	None predicted	135
mRNA_7629	102708	15,8	10,7	0,03	Oligopeptide transporter, OPT superfamily	IPR004813	819
mRNA_4861	103537	16,2	11,1	0,03	None predicted	None predicted	477
mRNA_9575	95515	15,7	10,7	0,03	Eukaryotic translation initiation factor 3 subunit J	IPR013906	275

UP_Vs_FV

mRNA	Protein	Value FV	Value UP	UP/FV	Interpro	Interpro	L (aa)
mRNA_5943	101889	12,1	18,6	91,23	Proteolipid membrane potential modulator	IPR000612	97
mRNA_712	119128	11,8	17,8	64,98	Large ribosomal subunit protein eL30-like	IPR039109	133
mRNA_9070	95791	12,8	18,1	41,10	CFEM domain-containing protein	IPR051735	171
mRNA_8309	96044	12,3	17,6	38,97	ATP synthase, F0 complex, subunit H	IPR019711	130
mRNA_1925	104308	11,9	17,1	36,01	Glycoside hydrolase, family 38	IPR000602	1084
mRNA_6350	103825	11,8	16,9	35,57	Cytochrome b-c1 complex subunit 8	IPR004205	104
mRNA_3600	96316	12,5	17,7	34,98	Proteasome, subunit alpha/beta	IPR001353	283
mRNA_9971	98135	11,8	16,8	32,14	Cytidine and deoxycytidylate deaminase domain	IPR002125	173
mRNA_1741	96097	11,8	16,8	31,65	SRP1/TIP1-like Cell Wall Component	IPR052982	249
mRNA_5149	103271	11,8	16,8	31,63	Mitochondrial outer membrane protein OM14	IPR039454	247
mRNA_19	95598	12,5	17,3	27,98	Proteasome, subunit alpha/beta	IPR001353	205
mRNA_2928	75550	11,6	16,3	25,95	Glycoside hydrolase, family 65	IPR005195	981
mRNA_8438	86181	11,7	16,4	25,62	Fungal Secondary Metabolite SDRs	IPR051468	268
mRNA_7666	102378	11,2	15,8	24,46	Formyltetrahydrofolate deformylase	IPR004810	286
mRNA_9536	104272	15,8	20,5	24,32	Vacuolar protein sorting-associated protein 62	IPR009291	199
mRNA_6747	101436	16,7	21,2	22,77	O-methyltransferase COMT-type	IPR016461	460
mRNA_10099	96554	13,2	17,7	22,53	None predicted	None predicted	155
mRNA_5515	94392	12,1	16,5	20,89	Small nuclear ribonucleoprotein Sm D3	IPR034099	129
mRNA_760	103976	13,1	17,5	20,46	None predicted	None predicted	253
mRNA_2471	102455	11,6	15,9	20,25	Cellulose-degrading glycosyl hydrolase, family 3	IPR050288	883

mRNA	Protein	Value FV	Value UP	UP/FV	Interpro	Interpro	L (aa)
mRNA_2244	81067	17,0	10,6	0,01	Fucose-specific lectin	SSF89372	541
mRNA_2812	72433	16,7	10,8	0,02	Serine/threonine-protein kinases, AGC	IPR050236	1399
mRNA_2277	99784	15,9	10,7	0,03	CCHC-type Zinc Finger Nucleic Acid Binding	IPR051714	222
mRNA_1015	100914	16,6	11,5	0,03	Claspin	IPR024146	1326
mRNA_5953	95653	16,5	11,4	0,03	None predicted	None predicted	583
mRNA_7671	85751	15,4	10,6	0,04	None predicted	None predicted	426
mRNA_1835	114176	15,0	10,5	0,04	None predicted	None predicted	481
mRNA_5313	96128	19,8	15,4	0,05	High Mobility Group Box (HMGB)	IPR050342	97
mRNA_9264	73539	15,4	11,0	0,05	Non-classical export protein 1	IPR024242	51
mRNA_2790	98508	17,0	12,6	0,05	Translocation protein Sec62, ascomycota	IPR011553	402
mRNA_3781	80264	14,9	10,6	0,05	None predicted	None predicted	410
mRNA_4146	97597	17,1	12,9	0,05	None predicted	None predicted	92
mRNA_4957	101746	15,0	10,9	0,06	None predicted; Helicase domain	IPR001650	1348
mRNA_8176	96568	15,0	10,9	0,06	U4/U6 small nuclear ribonucleoprotein Prp3	IPR027104	491
mRNA_847	97164	18,8	14,7	0,06	Eisosome component PIL1/LSP1	IPR028245	346
mRNA_7026	70123	15,7	11,6	0,06	Heh2/Src1-like	IPR044780	680
mRNA_2369	95389	15,7	11,6	0,06	Translation machinery associated TMA7	IPR015157	68
mRNA_8196	98545	15,6	11,5	0,06	Exocyst complex component Exo84	IPR033961	677
mRNA_6329	97161	15,0	11,0	0,06	Transcription elongation factor, IIS-type	IPR035100	298
mRNA_8331	91377	17,5	13,4	0,06	MYB Transcription Factor	IPR050560	252

Top20 UpReg

Top20 DwReg